Monthly Notices
of the
ROYAL ASTRONOMICAL SOCIETY

MNRAS **496,** 3512–3530 (2020)
Advance Access publication 2020 June 9

doi:10.1093/mnras/staa1618

Modelling the 3D climate of Venus with OASIS

João M. Mendonça ★† and Lars A. Buchhave

National Space Institute, Technical University of Denmark, Elektrovej, DK-2800 Kgs. Lyngby, Denmark

Accepted 2020 May 23. Received 2020 May 22; in original form 2019 August 9

ABSTRACT

Flexible 3D models to explore the vast diversity of terrestrial planets and interpret observational data are still in their early stages. In this work, we present OASIS: a novel and flexible 3D virtual planet laboratory. With OASIS we envision a platform that couples self-consistently seven individual modules representing the main physical and chemical processes that shape planetary environments. Additionally, OASIS is capable of producing simulated spectra from different instruments and observational techniques. In this work, we focus on the benchmark test of coupling four of the physical modules: fluid dynamics, radiation, turbulence, and surface/soil. To test the OASIS platform, we produced 3D simulations of the Venus climate and its atmospheric circulation and study how the modelled atmosphere changes with various cloud covers, atmospheric heat capacity, and surface friction. 3D simulations of Venus are challenging because they require long integration times with a computationally expensive radiative transfer code. By comparing OASIS results with observational data, we verify that the new model is able to successfully simulate Venus. With simulated spectra produced directly from the 3D simulations, we explore the capabilities of future missions, like LUVOIR, to observe Venus analogues located at a distance of 10 pc. With OASIS, we have taken the first steps to build a sophisticated and very flexible platform capable of studying the environment of terrestrial planets, which will be an essential tool to characterize observed terrestrial planets and plan future observations.

Key words: hydrodynamics – methods: numerical – planets and satellites: atmospheres – planets and satellites: terrestrial planets.

1 INTRODUCTION

1.1 Background

The research field of planetary sciences has significantly broadened its reach and scope in the last two decades with the discovery of a multitude of planets orbiting other stars. There are more than 4000 exoplanets known but the variety of environments that they may harbour is still unknown. Most importantly, it propels the fundamental scientific and philosophical quest of searching for the first detection of life beyond our own planet. Recently, results from the *Kepler* Space Telescope suggest that there are at least two Earth-sized planets orbiting every M-dwarf star (Dressing & Charbonneau 2015), which are the most abundant stars in our galaxy. M stars are colder and less massive than our Sun, which allows planets lying closer to their parent star to still retain atmospheres, and in some cases, to have the right conditions to host liquid water at their surfaces (Forget 2013). Being closer to their stars also facilitates probing their atmospheres with current observational methods. Recently, terrestrial planets orbiting M stars with potential habitable conditions have been detected, such as the TRAPPIST-1 planet system (Gillon et al. 2016, 2017; Luger et al. 2017), Proxima Centauri b (Anglada-Escudé et al. 2016), LHS 1140b (Dittmann et al. 2017), and Ross 128b (Bonfils et al. 2018). Space missions such as the *James Webb Space Telescope* (*JWST*), which will be launched in 2021, will be able to detect water features in the atmosphere of, for example, Earth-sized planets around M-dwarf stars (Morley et al. 2017; Batalha et al. 2018; Lustig-Yaeger, Meadows & Lincowski 2019; Wunderlich et al. 2019). However, a theoretical framework is needed to support these observations. Otherwise, the observational data may not be correctly interpreted, causing the community to miss possible habitable planets or erroneously identify barren planets as habitable. Furthermore, without a theoretical guide to select planet candidates, valuable observational resources may be wasted on planets, which theoretically are unlikely to harbour life.

Meaningful characterizations of planetary environments will require a large effort from theory and observations. Our chances of finding habitable planets and tracers of life may be increased if we effectively optimize the telescope observing time to target the most likely habitable planets and if we are able to accurately

★ E-mail: joao.mendonca@space.dtu.dk
† Homepage: software-oasis.com

interpret the ensuing observational data. The best targets are planets with long-term stability in their environment allowing liquid water at the surface (usually defined as habitable conditions, e.g. Forget 2013). This requires robust knowledge of the time evolution of planetary climates. To understand how planet environments evolve, we need to characterize the main mechanisms driving the climate and to explore the interplay of the chemical and physical processes using numerical models.

The characterization of exoplanet environments will be accomplished via remote sensing, where the theoretical platforms will have an important role interpreting the planet spectra and variations of the observed signals. Planetary environments can be very complex and a deep understanding of climate problems often requires a hierarchy of theoretical models. This is necessary due to the difficulty in interpreting results that are mostly associated with the intrinsic nonlinear nature of the problems. Such a hierarchical strategy allows us to gather important information on the assumptions, concepts, and limitations of the models developed. At the end of this hierarchy of models, we have the 3D global circulation models (GCMs). In this work, we focus on this last category. GCMs are powerful tools that include self-consistent representations of the main physical and chemical processes that drive the planet's environment (e.g. Donner & Large 2008). GCMs allow researchers to study the dynamical transport of heat, chemistry, and clouds across the 3D atmosphere. These advantages allow us to more accurately obtain the global temperature of planetary atmospheres. Several works have shown that 3D effects, such as a variation of the planet's albedo due to the sensitivity of the atmospheric circulation and the substellar cloud deck to the planet's rotation rate (Kopparapu et al. 2016), or the cold trapping of volatiles in the permanent night side of tidally locked terrestrial planets (Leconte et al. 2013) are important to understand the planet's environment. The heat transport in the atmosphere of tidally locked planets (these planets have permanent day–night sides) can have a very strong impact on the planet's environment, which in the case of inefficient heat transport can lead to atmospheric collapse (e.g. Wordsworth 2015). The terrestrial planets around low-mass stars in the habitable zone are potentially in a tidally locked state and the exploration of the heat transport in these scenarios cannot be done self-consistently with 1D models. Due to these features, 3D GCMs are one of the best and most reliable tools to study the environment in these planets. The observed data contain inherently 3D information on the planetary atmospheres that can be misinterpreted by simpler 1D models, which are unable to robustly represent the impact of the atmospheric circulation. Recently, Caldas et al. (2019) showed that day–night thermal and compositional contrast in tidally locked planets can produce a gradient in opacities that has an important impact on the planet spectrum. Data from thermal emission and reflectance spectra will also be strongly modulated by 3D effects caused by longitudinal differences in, for example, temperature, cloud cover, and surface/oceans. There is a long list of works that have used GCMs to study terrestrial planets with different levels of complexity (e.g. Shields 2019). The terrestrial planets studied with GCMs range from our own Earth, to planets in our Solar system and beyond. The diversity of studies used to explore planetary environments using 3D climate models include, for example, faint young Sun paradox on Earth and Mars (e.g. Charnay et al. 2013; Wolf & Toon 2013; Wordsworth et al. 2017), planetary snowball episodes (e.g. Abbot & Pierrehumbert 2010), Mars atmosphere (e.g. Forget et al. 1999), Venus atmosphere (e.g. Lebonnois et al. 2010; Mendonça & Read 2016), Titan atmosphere (e.g. Charnay et al. 2015), Pluto atmosphere (e.g. Forget et al. 2017), or evaluate the climate of terrestrial exoplanets (e.g. Wordsworth et al. 2011; Leconte et al. 2013; Shields et al. 2016; Turbet et al. 2017; Haqq-Misra et al. 2018; Del Genio et al. 2019; Komacek & Abbot 2019). GCMs to study terrestrial climates have also included the effect of atmosphere–ocean coupling, and have shown that ocean dynamics play an important role in the characterization of planet climates in the middle range and outer edge of the habitable zone (e.g. Yang et al. 2019). The disadvantage of GCMs against other simplified models such as the 1D radiative-convective models, is the heavy computations required for the 3D calculations. However, progress has been made to boost the performance of 3D calculations such as the implementation of the 3D code to run on graphic processing units (GPUs) that benefits from the GPUs massively parallel architecture (Mendonça et al. 2016).

Upcoming missions will offer exciting opportunities to implement new techniques to characterize terrestrial planets and search for habitable atmospheres. Combining robust theoretical platforms and observations will be essential to formulate the best methods for the first rigorous characterization of terrestrial planets.

1.2 Motivation

With the aim of exploring the large diversity of possible terrestrial climates, we are currently developing the platform OASIS.[1] OASIS is a 3D virtual lab that will include the representation of the main physical and chemical processes that shape planetary climate and their evolution. The new platform has been written completely from the ground up to avoid approximations that could compromise the flexibility of the model to explore a large diversity of planetary conditions. The model has also been developed to run on GPUs in order to be very efficient exploring a large parameter space of planetary characteristics, using complex and computationally expensive physical/chemical routines, and be able to do long time integrations. We are also developing tools that will use the 3D OASIS output to simulate the observed spectra for different observational methods. Our goal is for this platform to play a key role in helping the exoplanet community identify important targets for follow-up observations.

In this work, our goal is to present the first results of our new platform. We focus mainly on the coupling between the dynamical core (THOR), atmospheric turbulence (LOKI), surface/soil thermodynamics (ATLANTIS), and the radiative transfer (CYCLOPS). The numerical methods in these four modules are benchmarked in this work by computing the 3D Venus-like environment. As we explain later, the aim of OASIS is to include more self-consistent physical and chemical schemes, such as cloud formation and atmospheric chemistry. However, the representation of clouds and chemistry in this work is very simplified (the model assumes that the cloud cover and atmospheric composition are constant as a function of time). Our goal is not to tune the model to simulate accurately the Venus atmosphere, but to select the main Venus bulk parameters, and test whether our numerical model can reproduce the main properties of the Venus atmospheric circulation and temperature structure without further input. By exploring the atmosphere of Venus, we test OASIS with the most computationally challenging terrestrial planet to simulate in our Solar system. To be able to simulate Venus, the numerical models must be able to simulate the global atmosphere for thousands of Earth days until the model

[1] Recent news and updates on the OASIS platform can be found in www.software-oasis.com.

converges to a steady state (e.g. Lebonnois et al. 2010; Mendonça & Read 2016). The long integration is related to the large thermal inertia of the atmosphere that is weakly forced by stellar radiation (just about 2.5 per cent of the incoming stellar radiation reaches the surface (e.g. Tomasko et al. 1980; Mendonça et al. 2015). The radiation processes play an important role driving the dynamics and climate. To accurately represent the radiative processes in Venus, it requires a computationally expensive radiation transfer scheme due to the optically thick massive atmosphere that is covered with highly reflective clouds (e.g. Eymet et al. 2009). The radiation scheme also needs to be able to represent well the spectral windows that allow a more efficient energy exchange between the deep atmosphere and the upper layers above the clouds.

The challenging problems pointed out above set Venus as a good benchmark test to the coupling between the dynamical core (THOR), atmospheric turbulence (LOKI), surface/soil thermodynamics (ATLANTIS), and the radiative transfer (CYCLOPS). We also want to explore the impact of some important model parameters on the simulated atmospheres (cloud cover, atmospheric heat capacity, and surface friction). Having a robust model for Venus allows us to have confidence when characterizing Venus-like planets. Transit detections favour planets orbiting closer to the stars (e.g. Kane & von Braun 2008; Kane, Kopparapu & Domagal-Goldman 2014), which may be an indication that we will find more planets with atmospheric conditions similar to Venus than similar to Earth or Mars. Also, exploring Venus-like planets allows us to learn more about the inner edge of the habitable zone, and improve our understanding on the climate evolution of Earth and Venus.

Our long-term goals are to transform OASIS into a platform capable of modelling the atmospheric composition and evolution of terrestrial planets, and understand the key physical processes behind the diversity of planetary environments.

1.3 Venus

Venus is the most Earth-like planet in the Solar system in terms of mass and size. However, the current state of both planetary environments is very distinct. If the two planets started with similar planet conditions, different processes shaped distinct climate evolutions: stronger incoming stellar radiation in Venus (closer to the Sun), no magnetic field in Venus that makes atmospheric escape more efficient, and lack of a geochemical cycle in Venus that could remove volatiles such as CO_2 into the planet's interior. The state of the early Venus climate is still controversial due to lack of observational constraints and robust theory to support different scenarios. Some studies suggest that early Venus had a temperate climate that allowed liquid water to be stable at its surface, and that the planet lost all its oceans to the atmosphere during a net positive feedback between the surface temperature and the atmospheric opacity that enhances the strength of the greenhouse effect (Ingersoll 1969). Another possibility is that early Venus had a massive steam-filled atmosphere where the water could never condense at its surface (Lebrun et al. 2013).

The current Venus has a massive atmosphere composed mostly of CO_2 that creates a hostile environment at its surface: temperatures reaching roughly 735 K and pressure 92 bars (Taylor, Svedhem & Head 2018). 96.5 per cent of the dense atmosphere is CO_2 and 3.5 per cent N_2 including minor tracers such as 30 ppm of H_2O and 150 ppm of SO_2. The large quantity of CO_2 is responsible for the large temperatures obtained at the surface ('greenhouse' phenomenon, Sagan 1961). Other minor constituents in the atmosphere of Venus have been observed such as water, sulphur dioxide, and carbon monoxide (Taylor et al. 2018). The planet is completely covered by clouds that have a big impact on the energy budget of the atmosphere. Venus' clouds are mostly a mixture of sulphuric acid and water droplets, extending from an altitude of ∼45–65 km, with layers of sub-micron particles below and above the main cloud deck (Knollenberg & Hunten 1980). The clouds of Venus reflect most of the incoming stellar radiation back to space (the bond albedo is ∼0.75), and are very opaque in the UV, visible, and most of the infrared (IR) wavelength range (Read et al. 2016). However, there are some visible and near-IR spectral windows that have been used to observe the Venus lower atmosphere (e.g. Allen & Crawford 1984). There is a strong absorber in the cloud region in the UV range. This absorber is easily detected in the Venus UV images due to its effective absorption and inhomogeneous spatial distribution across the atmosphere (e.g. creates a horizontal 'V' shape structure across the atmosphere). The composition of this UV absorber is still not confirmed and some of the proposed identities of the unknown UV absorber are for example: sulphur aerosols, $FeCl_3$ (Krasnopolsky 2017), sulphur oxide isomer (OSSO, Frandsen, Wennberg & Kjaergaard 2016) or even organic components (Limaye et al. 2018). The UV absorber has also an important role in the deposition of stellar energy across the atmosphere.

Venus has almost no seasons (the spin inclination axis is ∼2.64°) and an orbital eccentricity around 0.007. The solid planet rotates slowly in a retrograde direction, and takes roughly 240 d to complete a full revolution (Carpenter 1964; Goldstein 1964). Despite the solid planet rotating slowly, the atmosphere is rotating faster in a phenomenon called superrotation. The cloud deck is estimated to take on average 4–5 Earth days to rotate around the planet (50–60× faster than the solid planet). The winds reach speeds of 100 m s^{-1} in the cloud region, and the mechanisms for their formation are described in Lebonnois et al. (2010) and Mendonça & Read (2016) as a combination of zonal mean circulation, thermal tides, and transient waves, where the semidiurnal tide plays a crucial role transporting angular momentum mainly from the upper atmosphere towards the cloud region. The superrotation index (S) or Read number quantifies the magnitude of the superrotation phenomenon in a planetary atmosphere, which is defined by the excess of total angular momentum of the atmosphere (M_t) compared to an atmosphere corotating with the solid planet (M_0):

$$S = \frac{M_t}{M_0} - 1. \quad (1)$$

Equation (1) was first defined in Read (1986). Mendonça & Read (2016) estimate from observational wind measurements (Kerzhanovich & Limaye 1985) a Read number of $8.7^{+5.2}_{-4.6}$ for Venus. Further details on how to compute the Read number can be found in Read (1986) or Mendonça et al. (2018).

1.4 Structure of this study

In this paper, we present the structure of what will be the OASIS platform and the first tests on the different modules working together. In Section 2, we present the different physics modules at work in OASIS. In Section 3, the results of the reference simulations with different spatial resolutions are presented and discussed. The results of the reference simulations are compared against the observations in Section 4. In Section 5, we perform sensitivity tests to the reference simulation where we explore a different cloud cover (5.1), atmospheric heat capacity (5.2), and surface friction (5.3). In Section 6, we move our simulated Venus planet to orbit a Sun-like

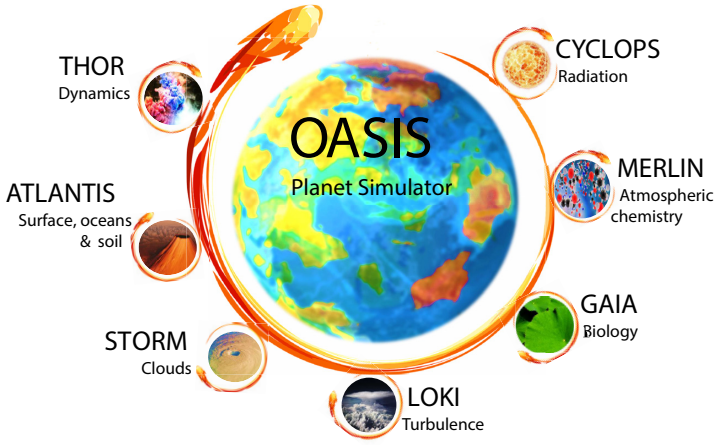

Figure 1. The architecture of the OASIS platform. The different modules around OASIS represent the different physical and chemical processes of the 3D platform: THOR represents the dynamical fluid flow in the atmosphere; CYCLOPS the interaction of the radiation with the atmosphere and surface; LOKI the turbulence in the atmosphere; STORM the cloud physics; ATLANTIS the mechanical interaction between the atmosphere and the surface, and the thermodynamics of the planet soil; MERLIN represents the atmospheric and surface chemistry; and GAIA is planned to be a module that will represent the effects of biology on the surface planet and on its atmosphere.

star at 10 pc away, and explore the results using an instrument with capabilities similar to the LUVOIR mission concept. Finally, in Section 7, we discuss our model results and future perspectives.

2 OASIS – A DEDICATED PLANETARY MODEL

OASIS is a new theoretical platform developed to expand our knowledge of planetary environments. The novel planetary virtual lab is aimed to couple self-consistently seven modules (Fig. 1) that represent physical and chemical processes in the planets, and it can be used as a fast 1D model (see the MIRAGE module below) or full 3D. This platform is part of a long-term project that gradually will include more physically based and complex parametrizations, and also model options to control the complexity of the model.

In the core of OASIS is THOR (Mendonça et al. 2016) – a module that includes a state-of-the-art dynamical solver, which represents the atmospheric fluid flow. Coupled self-consistently with THOR, we have currently three physical modules and three that are currently being developed:

Completed

CYCLOPS represents the absorption and scattering in the atmosphere and surface.

LOKI parametrizes the small-scale physics that requires very fine space and time resolutions to be fully represented (e.g. turbulence).

ATLANTIS represents the physics at the planet surface, soil, and the impact of the surface boundary in the atmosphere.

Under development

STORM incorporates our physical scheme for cloud formation and transport.

MERLIN solves the chemical equations in the atmosphere and surface.

GAIA is a module that is currently being developed and includes the manifestation of the presence of biology in the planet atmosphere and surface.

OASIS is being gradually improved in terms of code performance, usability and complexity in the physical/chemical modules. OASIS has a modular configuration that allow us to select the parts of the code that we want to include in the simulations. In the next subsection, we describe the current content of each completed modules and assumptions about gas composition and clouds. Note that the module names in OASIS do not correspond to acronyms. The main purpose of the module names is to allow the model user to easily remember the existing different model options and to highlight that each module can work as a stand-alone code or integrated to work together with other modules.

2.1 Completed modules

2.1.1 THOR – dynamical core

THOR is a state-of-the-art atmospheric dynamical core that solves the three-dimensional non-hydrostatic Euler equations on a modified icosahedral grid (Mendonça et al. 2016; Deitrick et al. 2020). The core architecture of OASIS is developed around this novel model. THOR is part of the Exoplanet Simulation Platform[2] (ESP) tools, and it can be downloaded at https://github.com/exoclime. The main advantages of using THOR against other recent planetary models is that:

(i) The atmospheric fluid flow is completely represented, and no approximations are used that could compromise the physics. In this work, THOR solves the 3D non-hydrostatic compressible Euler equations on a rotating sphere (Mendonça et al. 2016). THOR uses the horizontally explicit vertically implicit (HEVI; Satoh 2002) method to allow an increased integration time-step that would otherwise be constrained by fast sound waves.

(ii) The equations are solved on an icosahedral grid that avoids the problem associated with the convergence of the meridians at the poles in latitude–longitude grids.

(iii) The interface is user-friendly and can be easily adapted to a multitude of atmospheric conditions.

[2]ESP has a variety of atmospheric tools open source, such as: VULCAN: chemical kinetics for atmospheres (Tsai et al. 2017); HELIOS: radiative transfer code (Malik et al. 2017, 2019); HELIOS-R: nested sampling atmospheric retrieval code (Lavie et al. 2017); HELIOS-T: atmospheric retrieval code for exoplanet transmission spectra (Fisher & Heng 2018).

Table 1. Reference spectral resolution used in the 3D simulations.

Spectral range (μm)	Spectral resolution (μm)
1.70–2.55	0.02
2.55–22.75	0.1
40.75–100.75	10.0
100.75–260.75	40.0

(iv) It was developed to run on GPUs. The main advantage of using GPUs is the highly parallel architecture.

We have worked on a few upgrades to boost the performance of THOR, and the Venus-like simulations presented in this work using OASIS (including e.g. THOR and a full radiation scheme) take roughly 9 d using one NVIDIA V100 32GB graphic card. Other updates in the code are the inclusion of the radiative heating/cooling terms and wind friction from the physics modules directly into the dynamical equations (e.g. Deitrick et al. 2020). This update improves the stability of the model.

2.1.2 CYCLOPS – *radiative transfer*

CYCLOPS is a fast radiative parametrization that represents the absorption/emission/scattering by gases and clouds. The radiative transfer scheme is the most computational expensive routine in OASIS. Our code is based on the work developed in Mendonça et al. (2015). The stellar radiation calculations are based on the delta-Eddington approximation (two-stream-type) with an adding layer method (multiple scattering). For the thermal radiation case, the code is based on an absorptivity/emissivity formulation. More details on the equations solved can be found in Mendonça et al. (2015). The formulation is now implemented to work on GPUs, which allowed us to make the code in Mendonça et al. (2015) more flexible and accurate. In the current code (CYCLOPS), we do not degrade the resolution of the cumulative probability function, which was done before to boost the performance of the radiative transfer code. Our radiation code is now fully integrated over 353 spectral bands and 20 Gaussian points, using the complete information of the original *k*-distribution table and avoiding any tunable parameters. The spectral resolution of the *k*-table changes as a function of spectral ranges, and we show those different resolutions in Table 1. To boost the performance of the angular integration of the radiative transfer integration (emission solution), we have applied a three-point Gaussian quadrature integration instead of the typically used diffusivity factor. Our angular integrations increase the model flexibility and robustness.

The interaction of the radiation and air molecules depend largely on the molecular absorption cross-sections. In our work, we have used the code HELIOS-K to calculate the molecular opacities (Grimm & Heng 2015). We have applied a few changes to HELIOS-K to be able to produce opacities compatible with other works that have studied Venus (e.g. Lee & Richardson 2011): (i) extended the code to include the CO_2 line shape suggested in Meadows & Crisp (1996); (ii) used the data and methods from Gamache et al. (2017) to calculate the total internal partitions of the molecules; and (iii) after the line-by-line information is gathered we use a MATLAB routine to tabulate the optical data using the methods from Lacis & Oinas (1991). The molecules included in our study are CO_2, H_2O, and SO_2, which are the main molecules that contribute to the radiative budget in the atmosphere. For further details about the absorption line parameters explored in this work, please read Lee & Richardson (2011). The performance of our model was improved by building a unique *k*-table with the opacity of the three gases (CO_2, H_2O, and SO_2) across different temperatures and pressures. The concentration of each gas in the atmosphere was kept constant with time (see module MERLIN below).

We added an absorption continuum to the line-by-line absorption to represent the collision-induced absorption and to alleviate the limitation due to the far-wing line truncation. The collision-induced absorption is generated in the deep atmosphere due to the collisions between the molecules that induce dipole moments and that can behave momentarily like more complex molecules. We implemented the same approach as suggested in Lebonnois et al. (2015). The values to form the continuum were constrained from observations at fixed wavelengths: 0.7×10^{-9} cm^{-1} amg^{-2} at 1.18 μm (Bézard et al. 2011), 5×10^{-9} cm^{-1} amg^{-2} at 1.74 μm (de Bergh et al. 1995), and 3.5×10^{-8} cm^{-1} amg^{-2} at 2.4 μm (Marcq et al. 2006). As in Lebonnois et al. (2015), we have interpolated the absorption continuum between the spectral windows referred to above. Due to the lack of observational or experimental constrains to the absorption continuum, the uncertainties above 2.3 μm are large. Above 3 μm, we have added a base continuum of 3.0×10^{-7} cm^{-1} amg^{-2} similar to the value used in Lebonnois et al. (2015), which permits the model to calculate an average surface temperature of roughly 745 K. The collision-induced absorption values due to CO_2–CO_2 collisions at the wavelength range between 40 and 260 μm were taken from Gruszka & Borysow (1997) and Baranov, Lafferty & Fraser (2004).

We consider the Rayleigh scattering from CO_2 molecules, which is associated with the elastic scattering of light by particles (in this case molecules) that are smaller than the wavelength of the radiation. Rayleigh scattering is inversely proportional to the fourth power of the wavelength, and in our work we followed the parametrization from Haus, Kappel & Arnold (2015) to represent the scattering by CO_2 molecules.

As we explained in the Introduction and will discuss in Section 5.1, the cloud region in Venus contains an atmospheric constituent that causes a significant absorption of the stellar light at wavelengths between 0.32 and 0.8 μm. Despite the composition of the extra absorber is unknown, it is possible to constrain its spatial distribution and absorption efficiency from observations. We have implemented the same parametrization as in Haus et al. (2015), which allowed us to include the UV absorber without specifying its composition.

The cloud optical properties were calculated from Mie theory and made consistent with Crisp (1986). The composition of the cloud particles are assumed to be 25 per cent water and 75 per cent sulphuric acid, and the refractive indexes to calculate the optical properties of the clouds were taken from Palmer & Williams (1975). The surface reflectivity was set to 0.15 to represent the dark basaltic Venus' surface. You can read more about the Venus surface colour in Pieters et al. (1986).

The heating/cooling rates calculated from the radiative budget for each grid point have the following form:

$$Q = \frac{1}{\rho c_p} \frac{\mathrm{d}F_{\mathrm{rad}}}{\mathrm{d}z}, \tag{2}$$

where Q is the heating/cooling rates ($K\,s^{-1}$), ρ the atmospheric density ($kg\,m^{-3}$), c_p is the specific heat capacity ($J\,kg^{-1}\,K^{-1}$), and F_{rad} is the spectral integrated flux ($W\,m^{-2}$). F_{rad} contains the flux contribution from both short-wave and long-wave radiative schemes that are updated every 55 simulated hours and 4 h, respectively. The

quantity Q is inserted in the entropy equation solved in THOR, which then calculates the new updated temperatures in the atmosphere.

This code is very flexible and capable of exploring different atmospheric conditions and compositions. The main difficulty is to collect data that sufficiently well represent the optical properties at certain non-Earth-centric conditions (e.g. collision-induced absorption of CO_2).

The structure of CYCLOPS allows for a straightforward implementation of the dynamical-radiative-microphysical feedbacks on 3D simulations that will be explored soon with OASIS on Earth- and Mars-like atmospheres.

2.1.3 ATLANTIS – surface and soil

ATLANTIS is the physics module in OASIS that represents the surface and soil of planets. A future implementation will also have a representation of the oceans. In this work, we have set the Venus surface to be a flat basalt surface. The evolution of the soil temperature in our Venus simulation was calculated using the following equation:

$$\frac{\partial T}{\partial t} = -\frac{\lambda}{C}\frac{\partial^2 T}{\partial z_{\rm d}^2}, \tag{3}$$

where T corresponds to the different soil temperatures, C is the specific heat per unit volume, λ is the soil conductivity, and $z_{\rm d}$ is the depth length from the surface. We have used 11 layers to represent the soil in the planet. The multilayer soil formulation used is similar to the scheme developed in Warrilow, Sangster & Slingo (1986) and later used for the LMD Mars GCM (Hourdin et al. 1993) and Oxford Venus GCM (Mendonça & Read 2016). To represent the basalt soil thermal properties, we have set the thermal inertia of the surface/soil to be 2200 J m^{-2} K^{-1} s$^{-\frac{1}{2}}$ (Rees 1999). The formulation used allows us to also compute the radiative flux coming from the interior, which is then integrated in the energy budget of the surface to permit an accurate estimate of the surface temperature rate.

ATLANTIS also includes the planetary boundary layer that represents the interaction between the atmosphere and surface. The development of OASIS is built on physical modules with different levels of complexity to facilitate gaining physical intuition about all the processes working in the simulations. The simulations examined in this work include very simple schemes to represent the boundary layer. The mechanical interaction between atmosphere and surface is represented in the reference simulations by a Rayleigh friction scheme identical to the formulation proposed in Held & Suarez (1994) to represent the Earth boundary layer in Earth simulations:

$$\frac{\partial \mathbf{v}}{\partial t} = -k_v(\sigma)\mathbf{v}, \tag{4}$$

where $\mathbf{v}$ is the momentum and σ is the ratio of the atmospheric pressure over the surface pressure. k_v is the strength of the dissipation and it is modelled by

$$k_v = k_f \max\left(0, \frac{\sigma - \sigma_b}{1 - \sigma_b}\right), \tag{5}$$

where σ_b is set to 0.7 and k_f^{-1} is equal to 24 h. For simplicity, in this work, we use the same set of parameters proposed to represent the Earth's surface friction in our Venus simulations. In Section 5.3, we explore the impact of different dissipation strengths in the simulated atmosphere.

The excess of angular momentum observed in the atmosphere of Venus has to come from interchanges of angular momentum between the atmosphere and the surface (e.g. Mendonça & Read 2016). To improve the representation of this phenomenon in the simulations, we are testing more physically based formulations based on bulk transport turbulent mixing parametrizations (e.g. Mendonça & Read 2016; Read et al. 2017) for future works.

2.1.4 LOKI – turbulence

In LOKI, we include a representation of the small-scale physics that cannot be resolved in the 3D GCMs, namely, turbulence. Various physical phenomena are difficult to resolve in space or time in 3D atmospheric simulations, because they require prohibitively large computational resources. An alternative option is to recover their impact on the simulations by parametrizing their physical behaviour in the large-scale phenomena.

Convection occurs in the atmosphere when the temperature gradient becomes steeper than an adiabatic profile. The convectively formed instabilities have an important role mixing, for example, heat and momentum in the atmosphere. There is a diversity of parametrizations that have been implemented in climate models to represent the small-scale convection with different levels of complexity. In this work, we have implemented a simple routine that does not require any tuning. We have implemented a simple convective adjustment routine that has been used in other climate models, such as the LMD GCM (Hourdin et al. 1993). Our very efficient parametrization mixes the enthalpy instantaneously in a buoyant unstable atmospheric column. The equation solved is

$$\bar{\theta} = \frac{\int_{p_{\rm bot}}^{p_{\rm top}} C_p \theta \Pi dp}{\int_{p_{\rm bot}}^{p_{\rm top}} C_p \Pi dp} \tag{6}$$

where $p_{\rm top}$ and $p_{\rm bot}$ are the pressures at the top and bottom of the unstable column, and θ the potential temperature[3] (e.g. Mendonça et al. 2016). Note that in this parametrization the only physical quantity that is mixed is potential temperature; other quantities such as momentum remain fixed. The convection scheme is largely dependent on heat capacity, C_p, and we explore its impact on the simulation in Section 5.2.

Included in LOKI, we have a 'sponge layer' that prevents spurious wave reflections in the top rigid boundary that can compromise the stability of the numerical simulations and more importantly that can lead to erroneous results in the top most layers of the atmosphere. We followed the same formulation as explored in Mendonça et al. (2018). The scheme is formulated so that it attempts to represent wave breaking phenomenon in the atmosphere. We have formulated the code to linearly damp the eddy components of the momentum and temperature in the upper part of the atmosphere. The forcing increases with altitude and is limited to a shallow region in the top model domain. The formulation used also makes use of a very efficient method developed in Mendonça et al. (2018) to compute the eddy component of the wind from an icosahedral grid.

An essential numerical scheme to keep the atmospheric models stable is the numerical dissipation. Every model needs some type of dissipation to avoid the accumulation of high-frequency waves at the smallest scale resolved by the numerical model, mimicking the physical cascade of energy to smaller scales. The turbulence and eddy viscosity in the subgrid scale is represented by using a fourth-order hyperdiffusion operator coupled with a 3D divergence

[3]The potential temperature is the temperature that a parcel of dry air would attain if brought adiabatically from its initial state to a standard pressure (usually the surface pressure).

Table 2. Model parameters used in the baseline simulation of Venus.

Parameters	Venus	Earth	Units
Planet distance	0.7	1	au
Mean radius	6052	6371	km
Gravity (equator)	8.87	9.78	$m\,s^{-2}$
Gas constant	188	287	$J\,K^{-1}\,kg^{-1}$
Specific heat	900	1005	$J\,K^{-1}\,kg^{-1}$
Rotation rate	-2.99×10^{-7}	7.29×10^{-5}	s^{-1}

damping. The formulation is the same as used in Mendonça et al. (2016). We have also extended the original version from Mendonça et al. (2016), by implementing the vertical component of the divergence damping to make the divergence operator more homogeneous in 3D. However, this extra component did not have any impact on the results due to the still crude horizontal resolution compared to the vertical (the divergence damping strength scales with the spatial resolution). For more information on the technical details and implementation, please see Mendonça et al. (2016).

2.2 Prescription for gas composition and clouds

In this work, we use simple representations of the clouds and chemistry in Venus. Clouds play a very important role in the Venus' atmospheric circulation and climate. The cloud structure remains constant during the simulations. The cloud properties were constrained by Venus observations and are divided into three different particle size modes (Knollenberg & Hunten 1980; Crisp 1986): mode 1 corresponds to a mean particle size less than 0.4 μm and extend from 32 to about 90 km altitude; mode 2 particles have a mean size of 1 μm and form part of the main cloud deck from roughly 50–80 km altitude; the largest particles are included in the mode 3 with a mean particle radius of 3.65 μm and located between 50 and 60 km. We have included the composition of the four main gases in the atmosphere. The concentration of the different gases was assumed to be well mixed in the atmosphere and close to the defined in the Venus International Reference Atmosphere (VIRA, von Zahn & Moroz 1985). The CO_2 concentration is set to 0.965 vmr,[4] H_2O to 5×10^{-5} vmr, SO_2 to 1×10^{-4} vmr, and the rest in N_2. The concentrations are not meant to be exactly equal to the values observed but to capture the main bulk conditions of a Venus-like planet.

3 REFERENCE SIMULATIONS

The reference simulation tests include a complete coupling of THOR (dynamics), CYCLOPS (radiation), LOKI (turbulence), and ATLANTIS (surface and soil), with a constant cloud cover and chemical composition.

3.1 MIRAGE

The input to our simulations is shown in Table 2, and the composition of the atmosphere and surface, and the cloud parameters as described in the previous sections. Before OASIS starts running the 3D computations, a module called MIRAGE calculates the 1D radiative-convective solution from the set of planet parameters chosen by the modeller. The module MIRAGE combines the radiative transfer scheme with the convective adjustments and the soil codes. The MIRAGE computations are performed in a column of the 3D grid, which is only discretized vertically in altitude. The stellar flux is globally averaged according to Crisp (1989), and the simulations are integrated until the temperature in each grid cell converges to a steady value (radiative-convective solution). The global-averaged temperature–pressure profile obtained with the 1D MIRAGE module is later used to initialize the temperatures and pressures of every column in the 3D simulation (all the columns start with the same input). This procedure allows us to speed-up the convergence of the deep thermal structure in Venus-like planets where the radiative time-scales are hundreds of Earth days.

The module MIRAGE is also used to test new physical modules before implementing the 3D configuration, allow fast exploration of the planetary parameter space, and build a physical intuition on complex planetary climate problems. MIRAGE can reproduce the emission and transmission spectra from the 1D radiative-convective temperature profiles but those capabilities are not explored in this work.

3.2 3D reference simulations

OASIS has integrated the Venus simulations for 25 000 Earth days. The initial temperature in each column was set to the temperature–pressure profiles obtained from the MIRAGE module (as explained in the previous Section), and the initial wind speed is set to a solid body rotation with an equatorial maximum of 30 $m\,s^{-1}$. The initial wind structure helps the model to start from a more stable solution than starting from rest. It is important to note that it has been shown that the spin-up phase of the Venus simulations are roughly 25 000 Earth days (e.g. Lee, Lewis & Read 2007), which means that by the end of the simulations the initial states have been forgotten and the climate solutions converge to a statistical steady state. For the reference 3D simulations, we have run two simulations that started from the same initial conditions but with different spatial resolutions: roughly 4 and 2 deg. The two simulations used exactly the same input, however, the time-step of the 2 deg resolution was reduced to 50 s to satisfy stability criteria from the dynamical core THOR. Fig. 2 shows the zonal winds (longitudinal component of the wind field) and mass stream function at the end of the simulations.

The 4 deg model has 4 times fewer grid columns than the model with 2 deg, which results in a simulation roughly 4 times faster. The 4 deg simulation has obtained qualitatively the same climate features as the 2 deg simulation, however, quantitatively the magnitude of the equatorial jets and the meridional circulation are distinct. We find that the inability of the 4 deg spatial resolution simulations in producing the strong winds is associated with the numerical errors in the advection scheme that become comparable to the physical sources/sinks in the deep atmosphere (see e.g. Lebonnois et al. 2012 or Thuburn 2008 for a more detailed description on the conservation properties in dynamical cores). The amplitude of this error will vary for different methods used in the dynamical cores, which means that the threshold in spatial resolution is expected to vary for different models. However, despite the differences, both simulations obtain similar wind and temperature distributions. Both simulations with different spatial resolution show two regions of local maxima in the winds: at pressure levels near the cloud top (∼100 mbar) and in the lower atmosphere at pressures between 1 and 10 bars. In both resolution experiments, the model produced two shallow direct circulation cells within the 10 lowest kilometres. In the 2 deg simulation, the mass stream function shows, above this

[4]vmr – volume mixing ration.

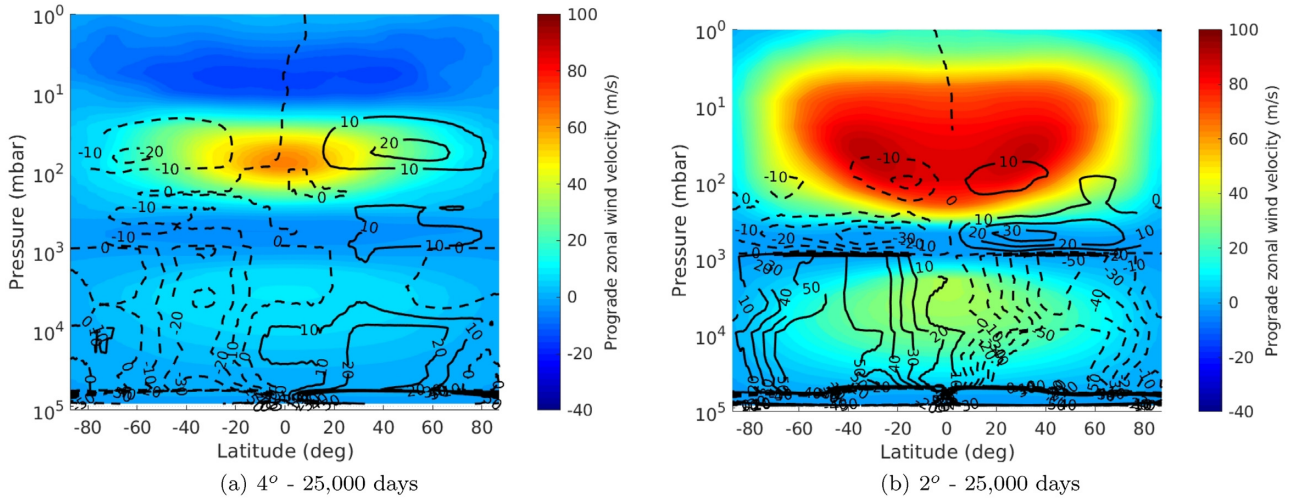

Figure 2. Zonally and timed averaged zonal winds and mass stream function for the reference simulation with different spatial resolution: (a) 4 deg and (b) 2 deg. The units of the zonal winds are in m s^{-1} and the positive numbers point in the prograde direction of the planet. The mass stream function is shown as the contours and is in units of 10^{10} kg s^{-1}. The results were averaged over 1000 Earth days.

region the formation of indirect cells that extend from the shallow direct cells to roughly 1 bar (roughly the pressure level of the cloud base in the simulations). The atmospheric circulation in the 4 deg simulation is more complex in the region between 10 and 1 bar: the zonal winds are weaker than the 2 deg simulations, and the mass stream function shows a complex pattern that evolves with time, similar to the results obtained in Mendonça et al. (2016). However, the atmospheric cells in this region tend to form large extended direct cells. Above the cloud base, the atmosphere is largely driven by the absorbed stellar radiation, and both simulations form large Hadley cells.

The global mean temperature for the reference simulations are shown in Fig. 4(a). The global mean temperature–pressure profiles for the simulations with different spatial resolutions are very similar, with a surface temperature of roughly 745 K. The temperature differences along the longitude in the upper atmosphere (above the pressure level 1 bar) are small as it shown in Fig. 3. The upper atmosphere is the region where the temperature differences are expected to be larger due to the small radiative time-scales and also because it is the region where most of the stellar radiation is absorbed. The small differences are associated with the efficient heat transport by the winds from the day to the night side. As we will see in Section 4, due to the small differences in temperature along the longitude, the differences between the IR spectra from day and night side are also very small. The amplitude of the diurnal and semidiurnal thermal tides in the atmosphere above the clouds are a few Kelvin, and similar to the results found in other GCMs such as Mendonça & Read (2016) and Lebonnois, Sugimoto & Gilli (2016).

The strong winds overlaying a slowly rotating planet set Venus on a cyclostrophic regime (e.g. Mendonça et al. 2012). In this regime, the centrifugal acceleration balances the geopotential gradient term (Leovy 1973), which links the temperature structure with the atmospheric circulation. In this approximation, a positive latitudinal gradient of the temperature is associated with a negative vertical gradient of the zonal winds. To clearly show the temperature structure as a function of latitude, in Figs 4(b) and (c) we show the temperature anomaly (T_a) maps. The anomalies were calculated

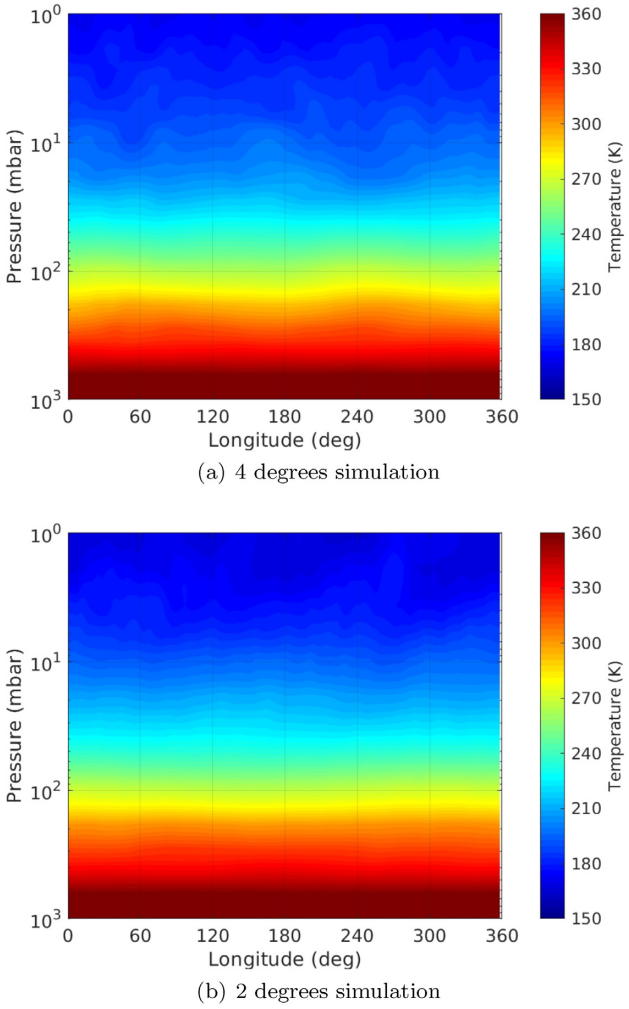

Figure 3. Temperature maps of the upper atmosphere along the equatorial region obtained at the end of the simulations with 4 deg (a) and 2 deg (b). The values were averaged in latitude between −20° and 20°.

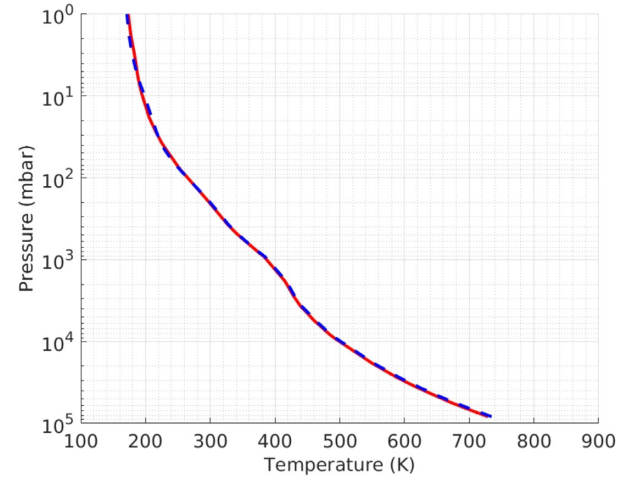

(a) Global mean temperatures

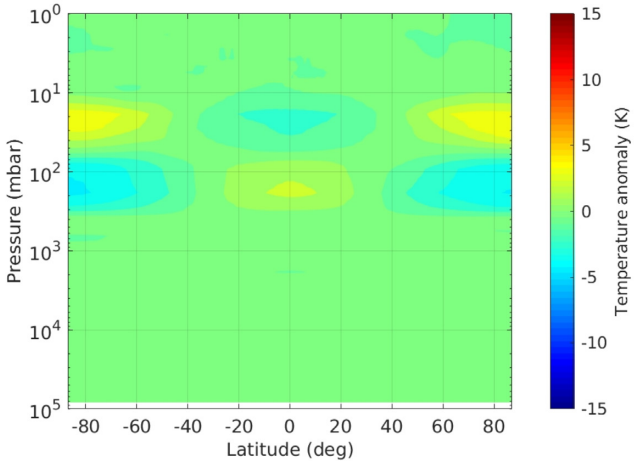

(b) 4 degrees simulation

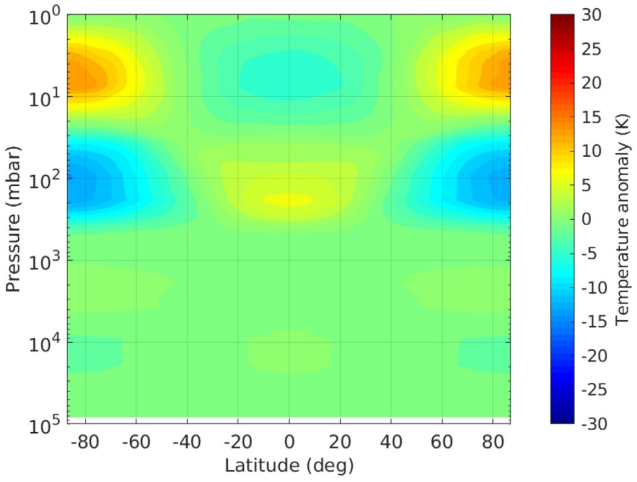

(c) 2 degrees simulation

Figure 4. (a) Map of the horizontally and time (1000 Earth days) averaged temperatures. The two lines represent the two simulations with different space resolution: the red solid line is the 4 deg simulations and the blue dashed line the 2 deg. (b) and (c) are the zonal and time averaged (over 1000 Earth days) temperature anomaly maps (see equation 7).

from the following equation:

$$T_{\rm a} = T - \frac{\int_{\lambda=0}^{\lambda=2\pi}\int_{\phi=-\pi/2}^{\phi=\pi/2} T A^2 \cos\phi \,{\rm d}\lambda\,{\rm d}\phi}{\int_{\lambda=0}^{\lambda=2\pi}\int_{\phi=-\pi/2}^{\phi=\pi/2} A^2 \cos\phi \,{\rm d}\lambda\,{\rm d}\phi}, \quad (7)$$

where T is the absolute temperature, A is the radius of the planet, ϕ is the latitude, and λ is the longitude. The hotter poles are produced by the compressional adiabatic heating caused by the downward branch of the large Hadley cells. The equator-to-pole differences are larger in the simulation with 2 deg resolution, which is associated with the stronger winds formed in this simulation. The temperature differences in the 2 deg simulation are between 20 and 30 K at 100 mbar, which is compatible with the observational work from Venus Express that shows equator-to-pole temperature differences of 30 K (Tellmann et al. 2009). However, at 1 bar the results based on observations (Tellmann et al. 2009) also show equator-to-pole temperature differences of 30 K, with a latitudinal gradient in the temperature starting at high latitudes (roughly 60° latitude), which is not reproduced in our simulations. Other Venus GCMs that used non-grey radiative transfer such as Lebonnois et al. (2010, 2016) and Mendonça & Read (2016), also underestimate the equator-to-pole temperature differences at 1 bar, which could be related with the poor representation of the cloud distribution across the atmosphere in the models. The 4 deg simulation obtained similar temperature anomaly pattern than the 2 deg simulation, however, the winds that have half of the absolute magnitude, produced equator-to-pole differences with roughly half of the temperature anomalies observed in the 2 deg simulation.

Despite the differences in the magnitudes between the simulations with 2 and 4 deg, both produce qualitative the same atmospheric circulation and temperature structure. The simulation with 4 deg is also similar to the simulations reproduced by Lebonnois et al. (2010) and Mendonça & Read (2016) that used similar physical modules but different dynamical core based on finite difference methods and a space resolution of 5 deg. Since we can capture roughly the same temperature structure and wind distribution of the 2 deg simulations with the 4 deg simulation, we decided to explore the impact of the clouds, different heat capacity of the atmosphere, and surface friction in the simulated atmospheres with the 4 deg set-up because simulation is 4× faster than the 2 deg simulation.

4 COMPARISON WITH OBSERVATIONS

The goal of this work was not to interpret new detailed data of Venus, or reproduce accurately the current Venus state, but to simulate the broad climate and circulation features that characterize Venus. However, as it is shown below, OASIS obtains robust results that reproduce quantitatively the temperature structure and circulation in Venus.

The global mean temperature from observations and the OASIS simulations are shown in Fig. 5. As we saw in the previous section, the two simulations with different resolution obtain almost identical global mean temperature profiles. The observational profile is based on the results presented in Kliore et al. (1985) (VIRA). There is good agreement between the model and observations, however, in the cloud region, the model results are consistently warmer than the observations. The temperature in this region is sensitive to the cloud distribution and parameters (Lebonnois et al. 2015), and we could have reduced the differences between the model results and the observations by tuning those parameters. However, finding the correct cloud distribution and parameters to match exactly the Venus

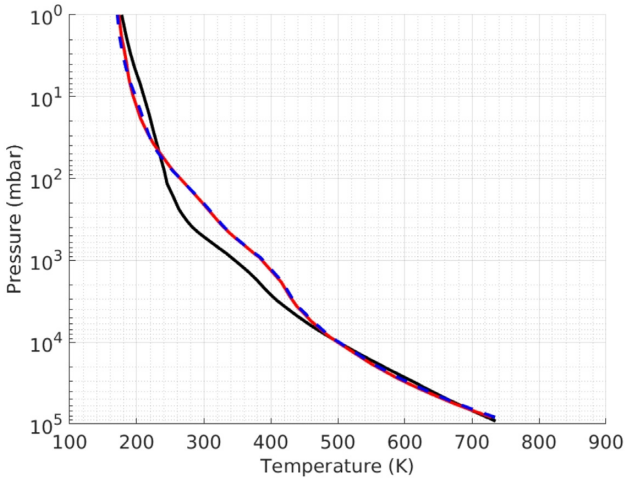

Figure 5. Global mean temperature from observations and OASIS. The solid black line is the VIRA (Venus International Reference Atmosphere) temperature profile based on observations of Venus (Kliore, Moroz & Keating 1985). The OASIS profiles overlap each other: blue dashed line (2 deg simulation) and red solid line (4 deg simulation).

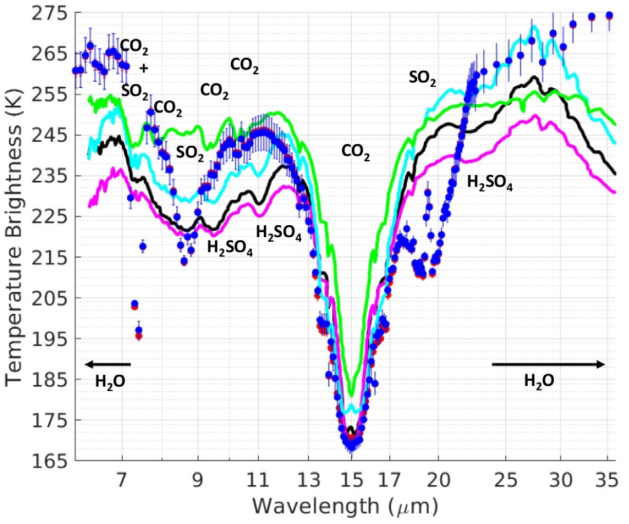

Figure 6. Brightness temperature from OASIS and observations from Venera 15 (Zasova et al. 2004). The solid lines are results from observations at different regions in the atmosphere (Zasova et al. 2004): (black solid line) latitude $<35°$, $L_s = 20$–$90°$; (magenta solid line) latitude $<35°$, $L_s = 270$–$310°$; (cyan solid line) $10° <$ latitude $< +10°$, $L_s = 75°$; (green solid line) North polar region, latitude $>85°$; where L_s is the solar longitude. The main absorption features from CO_2, H_2O, SO_2, and H_2SO_4 are indicated in the figure. The blue and red points are results from OASIS with a space resolution of 2 and 4 deg, respectively. The model results correspond to globally averaged values of the brightness temperature for different wavelengths. The uncertainties of the model values are the standard deviation of the globally averaged values.

current state goes beyond the scope of this paper. Our results are, for example, consistent with Lee & Richardson (2011) that used the same cloud distribution as we did (from Crisp 1986) and a more computationally expensive radiative transfer scheme from the model DISORT (Stamnes et al. 2000).

Fig. 6 shows the brightness temperature as a function of wavelength from OASIS and observations of Venus. The model results presented in Fig. 6 are at the same spectral resolution than the spectral resolution used in the OASIS simulations. The observational values were obtained from different missions and also at different locations in the atmosphere as explained in the caption of the figure. The brightness temperature is a measure of the upward IR radiance at the top of the atmosphere, and can provide information about the vertical temperature structure and composition of the atmosphere. There is a good agreement between the observed values and the OASIS results close to the centre of the CO_2 lines, for example, at 15 μm. The good representation of the model CO_2 line is associated with the temperatures of the upper atmosphere, above the cloud deck, being very close to the observed values. Note that there is almost no difference between the simulations with different resolution. The main differences between the model results and the observations are at the wavelengths of the SO_2 absorption lines, such as at around 7, 9, and 20 μm. In these regions, the brightness temperature from OASIS is consistently lower than the values observed. The differences with respect to the observations around the SO_2 features are expected since we have assumed a well-mixed SO_2 concentration in the atmosphere that is higher than the values observed in the Venus upper atmosphere (e.g. Taylor et al. 2018). The brightness temperature observed in Venus around the SO_2 lines corresponds to radiation coming mostly from the upper cloud region. On the other hand, by increasing the levels of concentration of SO_2 in our model, we see that the regions above the clouds, where the temperatures are colder, have a larger contribution to the brightness temperature. The higher values of SO_2 absorption in the upper atmosphere could be used in the future to explore signs of volcanic activity in other planetary atmospheres. The water features represent emission from the upper cloud region, and as we saw before in Fig. 5, the temperatures in the cloud region in our reference simulation are warmer than the observed values.

Venus is known to exhibit very strong atmospheric winds. Several different observational methods have been used to study the atmospheric circulation in Venus, however, the circulation below the cloud base continues poorly constrained observationally (e.g. Sánchez-Lavega et al. 2017). A very common method to measure the wind speed in Venus is based on cloud tracking of multiple temporal images. The cloud tracking method assumes that the cloud components behave as passive tracers of the atmospheric flow and allow to estimate the magnitude and direction of the horizontal winds. There is a large amount of data from cloud tracking measurements of the Venus atmosphere (e.g. Sánchez-Lavega et al. 2017) and we compare our model results with the observations from multiple space missions in Fig. 7. The results of the model and the observed values show clouds moving in Venus at a velocity around 100 m s^{-1}, which is roughly 60× faster than the rotational velocity of the solid planet. The simulation with 4 deg resolution obtained winds consistently weaker than the observations, and a large variability on the magnitude as evident from the large standard deviation. Notice that, as explained in Section 3.2, the main cause for the difference in the magnitude of the winds is the numerical precision in the advection scheme, which is improved when using better spatial resolution. The simulation with 2 deg reproduced strong winds that are largely consistent with the observations within the standard deviation. Despite the slightly weaker winds in the equatorial region, the model results represent the Venus circulation in the cloud region very well. This represents a great success for the OASIS platform since 3D GCM simulations of the Venus circulation are very challenging (Sánchez-Lavega et al. 2017).

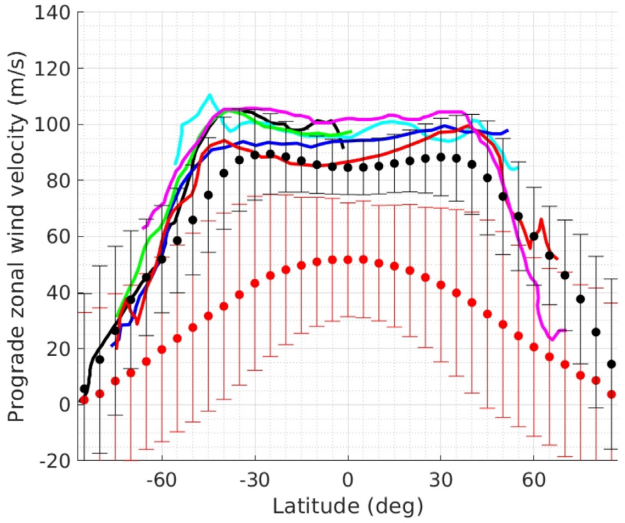

Figure 7. Zonal wind profiles from observations and the OASIS simulations. The winds plotted correspond to an altitude range of 65–70 km. The observational values were estimated by tracking the cloud motions at UV wavelengths in multiple space missions (Sánchez-Lavega et al. 2017): Mariner 10, 1974 (cyan solid line); Pioneer-Venus, 1980 (blue solid line); Pioneer-Venus, 1982 (red solid line); Galileo, 1990 (magenta solid line); Venus Express VIRTIS, 2006–2012 (black solid line); Venus Express VMC, 2006–2012 (green solid line). The filled circles correspond to the model results: red (simulation with 4 deg spatial resolution) and black (simulation with 2 deg spatial resolution). The model results were spatially averaged over the day-side hemisphere to be consistent with the UV observations and the uncertainties correspond to the standard deviation. The results were time averaged over 1000 Earth days.

5 SENSITIVITY EXPERIMENTS

The experiments in this section were integrated with a model configuration similar to the 4 deg reference simulation described in Section 3.

5.1 Clouds

The clouds in Venus have an important impact on the planet's energy budget and in its appearance. The presence of the clouds in the atmosphere causes a large fraction of the solar energy to be deposited in the cloud region, which has a strong influence on the waves excited in that region that drive the atmospheric circulation (e.g. Lebonnois et al. 2010; Mendonça & Read 2016). As explained in the Introduction, the clouds in Venus are a mixture of sulphuric acid H_2SO_4 and small amounts of H_2O (typically 25 per cent). In the cloud region, we also find a UV absorber which still has, as discussed in the Introduction, an unknown composition. In this section, we attempt to determine the impact of the unknown UV absorber and the clouds in the temperature and atmospheric circulation. Studying the case of a cloud-free Venus atmosphere is also interesting because Venus may have experienced periods of cloud-free events. The main component of the clouds, H_2SO_4, is produced photochemically from the photolysis of SO_2 and CO_2 (e.g. Catling & Kasting 2017). However, the abundances of SO_2 and H_2O are driven by the exospheric escape of hydrogen and heterogeneous reactions with surface minerals and volcanic outgassing. In Bullock & Grinspoon (2001), it is suggested that the Venus clouds would largely dissipate on a time-scale of 30 Myr without continued volcanic outgassing.

We run two simulations: one with H_2SO_4 clouds but no UV absorber, and another with no UV absorber or clouds. In Fig. 8, we investigate the main impact of the clouds in the temperature structure of Venus from our 3D simulations. Fig. 8(a) shows the global mean temperatures. The reference simulation described in the previous section is the red line. If the unknown UV absorber is removed from the simulations (green solid line in Fig. 8a) it affects the temperatures of the upper atmosphere, which becomes colder. The deep atmosphere is only slightly affected by a very small heating of the planet surface. If the clouds are completely removed (including the unknown UV absorber), it has a large effect in the temperature: the temperature in the upper atmosphere becomes similar to the case of just removing the unknown UV absorber (blue solid line in Fig. 8a), which is an indication that the unknown UV absorber has a larger impact on the temperatures of the upper atmosphere than the H_2SO_4/H_2O clouds; the lower atmosphere becomes much hotter, which is because the energy that was being reflected by the clouds is now reaching deeper regions in the atmosphere (including the surface). With no clouds, the atmosphere becomes considerably less opaque to the solar radiation in the 1–0.01 bar region, and scattering becomes less important to the atmospheric radiative budget. In this case, the atmospheric structure produced becomes similar to results found with a grey thermal radiative transfer (Robinson & Catling 2012) where the atmosphere develops a deep dry convective region that extends from the surface to roughly 0.1 bar. Figs 8(b) and (c) show the temperature anomaly maps from the two cloud experiments. If we remove just the unknown UV absorber, the amplitude of the temperature anomalies is weaker than the reference simulation, but their spatial distribution is similar. Removing the clouds completely has a large impact, and the anomalies become very small (Fig. 8c). Fig. 9 shows the winds produced by the cloud experiments. As expected, the winds produced by the case with no unknown UV absorber (Fig. 9a) are similar to the reference simulations, but produces weaker zonal winds. It is also worth noting that the atmospheric direct cells in the cloud region become stronger. The upper atmosphere becomes more transparent to the UV radiation causing a larger latitudinal gradient of the radiative heating in the lower cloud region and that induces the formation of stronger atmospheric cells. With no clouds (Fig. 9b), the zonal winds become very weak with a stronger meridional wind component. More energy is deposited in the deep atmosphere, which creates a more dynamically active lower atmosphere: multiple strong atmospheric cells are stacked on the top of each other. The stronger vertical mixing shown in the simulation with no clouds may have an important impact on the chemical spatial distribution for planets with similar characteristics. See the work of Lincowski et al. (2018) for a discussion on the impact of the clouds in the 1D radiative-convective equilibrium temperature profile for a planet with Venus-like composition around the TRAPPIST-1 star.

5.2 Atmospheric heat capacity

A constant heat capacity of the atmosphere is a good approximation for the Earth. However, in the massive Venus CO_2 atmosphere, the heat capacity has a strong dependence on the temperature, and can change from roughly 1200 $J\,K^{-1}\,kg^{-1}$ at the surface to 600 $J\,K^{-1}\,kg^{-1}$ at 100 km altitude. Other Venus GCMs have included the dependence of the heat capacity on the temperature (e.g. Lebonnois et al. 2010; Mendonça & Read 2016). To include the dependence of the heat capacity on the temperature in a GCM requires that some important quantities such as the potential temperature are re-formulated. As shown in Lebonnois et al. (2010) and Mendonça

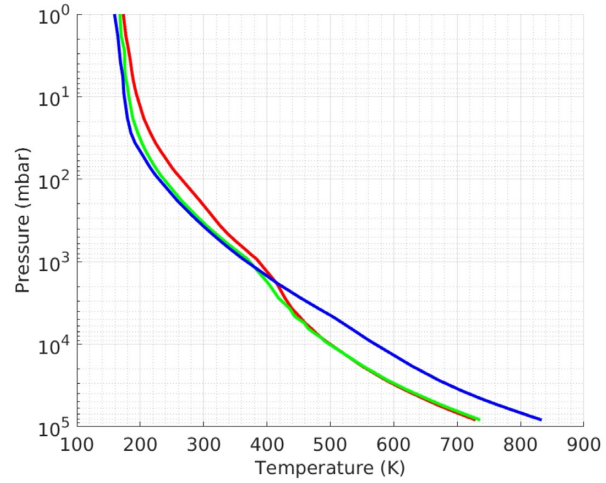

(a) Cloud experiments

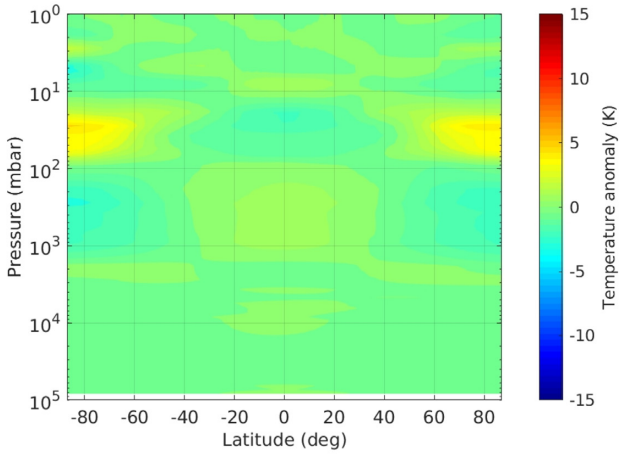

(b) No extra UV absorption

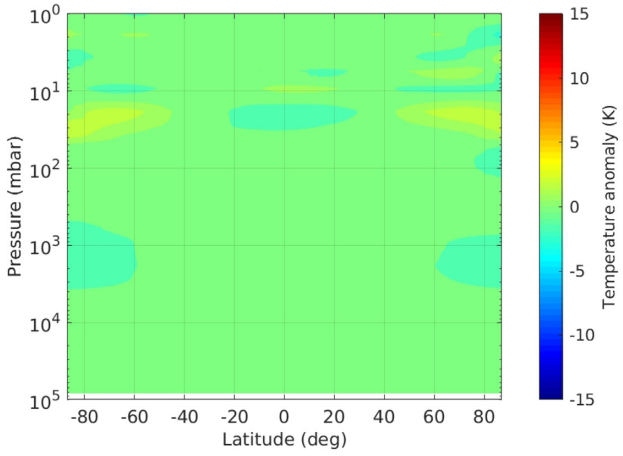

(c) No clouds or UV absorber

Figure 8. Temperatures obtained in the cloud experiments. (a) Map of the horizontally and time (1000 Earth days) averaged temperatures. The three coloured solid lines represent the three different experiments: green, no extra UV absorption; red, reference simulation; blue, no clouds or extra UV absorption. (b) and (c) are the zonal and time averaged (over 1000 Earth days) temperature anomaly maps (see equation 7).

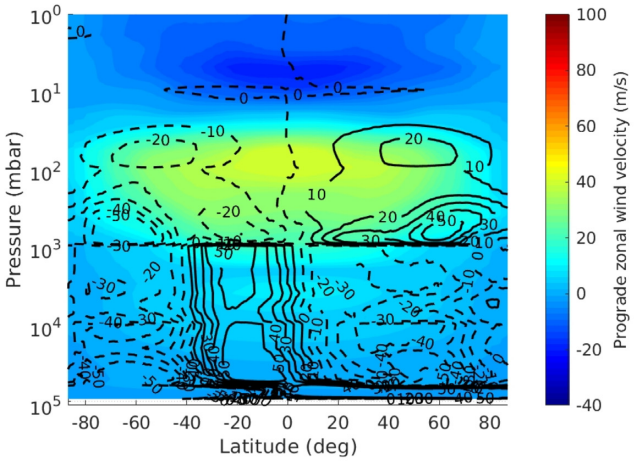

(a) No extra UV absorption

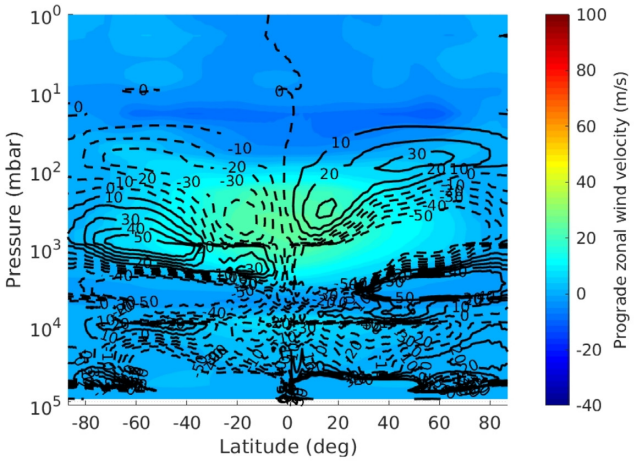

(b) No clouds and no extra UV absorption

Figure 9. Zonally and time averaged zonal winds and mass stream function for cloud experiments: (a) no extra UV absorption and (b) no clouds and no extra UV absorption. Both simulations use 4 deg spatial resolution and the results were averaged over 1000 Earth days. The units of the zonal winds are in $\mathrm{m\,s^{-1}}$ and the positive numbers point in the prograde direction of the planet. The mass stream function is shown as the contours and is in units of $10^{10}\ \mathrm{kg\,s^{-1}}$.

& Read (2016), the dynamical core of the GCMs (the part that solves the fluid equations) has to be modified to take this new formulation of potential temperature into account. More details on the implementation of a variable heat capacity in GCMs can be found in Lebonnois et al. (2010) and Mendonça & Read (2016). Other changes are easier to implement, such as the calculation of the radiative heating rates and convective adjustment. In Mendonça & Read (2016), the entropy was mixed in the atmosphere in a superadiabatic atmospheric column instead of the usually used enthalpy (in the subsection LOKI we describe the convective adjustment routine used in the current version of OASIS). In this work, we have decided to fix the value of the heat capacity. To test the impact of using different heat capacity values in the simulations we run two more simulations: heat capacity of 700 and 1100 $\mathrm{J\,K^{-1}\,kg^{-1}}$.

Fig. 10(a) shows the horizontal and time averaged temperatures of the three simulations: two with the different heat capacity values and the reference simulation. The profiles look very similar. The largest differences are located in the deepest atmosphere and the

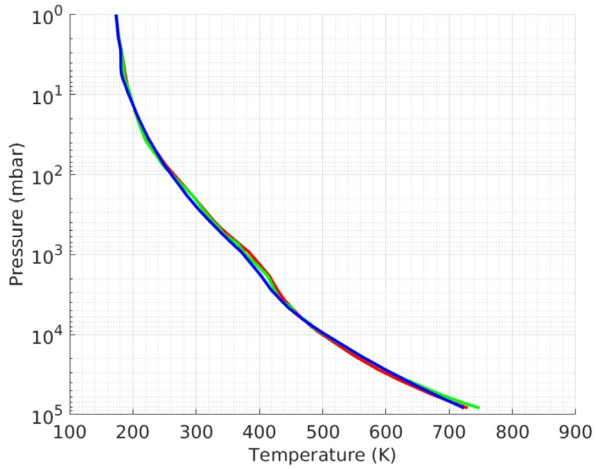

(a) Heat capacity experiments

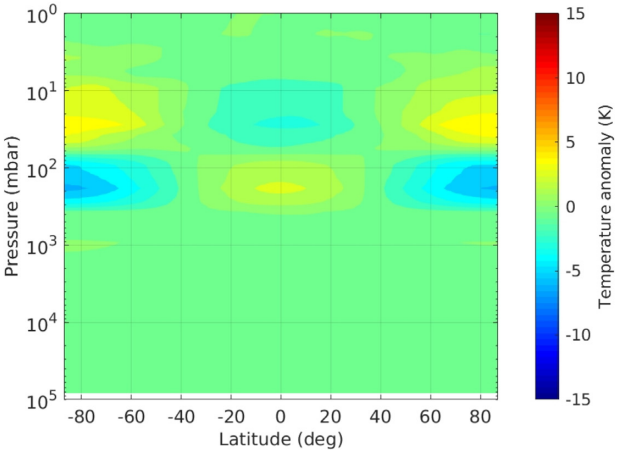

(b) Heat capacity equals to 700 J $K^{-1}kg^{-1}$

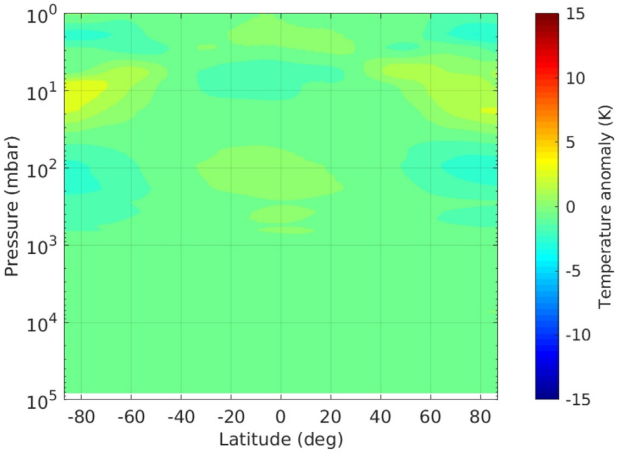

(c) Heat capacity equals to 1100 J $K^{-1}kg^{-1}$

Figure 10. Temperatures obtained in the heat capacity experiments. (a) Map of the horizontally and time (1000 Earth days) averaged temperatures. The three coloured solid lines represent the three different heat capacity values used: green, 700 J $K^{-1}kg^{-1}$; red, 900 J $K^{-1}kg^{-1}$; blue, 1100 J $K^{-1}kg^{-1}$. (b) and (c) are the zonal and time averaged (over 1000 Earth days) temperature anomaly for heat capacity of 700 and 1100 J $K^{-1}kg^{-1}$, respectively.

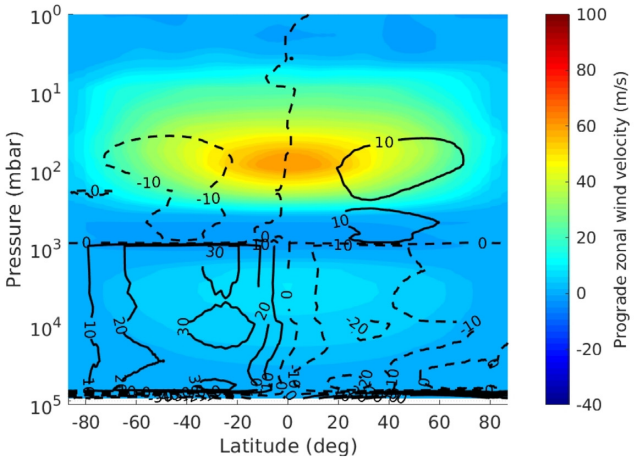

(a) Heat capacity equals to 700 J $K^{-1}kg^{-1}$

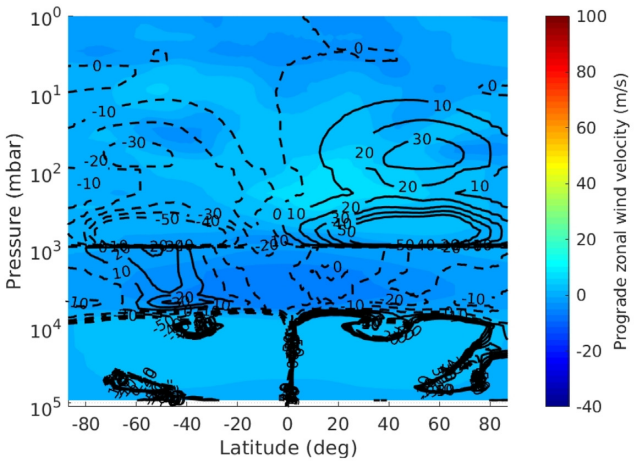

(b) Heat capacity equals to 1100 J $K^{-1}kg^{-1}$

Figure 11. Zonally and timed averaged zonal winds and mass stream function for simulations with different heat capacity values: (a) 700 and (b) 1100 J $K^{-1}kg^{-1}$. Both simulations use 4 deg spatial resolution and the results were averaged over 1000 Earth days. The units of the zonal winds are in m s^{-1} and the positive numbers point in the prograde direction of the planet. The mass stream function is shown as the contours and is in units of 10^{10} kg s^{-1}.

cloud region. There is almost no difference between the case with 900 and 1100 J K^{-1} kg^{-1} in the hot deep atmosphere, however, the case with 700 J K^{-1} kg^{-1} obtained a hotter surface. The hotter values are associated with less energy being transported vertically by convection, which allows the formation of a steeper lapse rate. Figs 10(b) and (c) show the temperature anomaly maps that are similar to the reference simulations. However, the anomalies in the simulation using 1100 J K^{-1} kg^{-1} are weaker than in the other experiments.

The winds produced in these experiments are shown in Figs 11(a) and (b). The wind pattern and strength in the simulation with heat capacity of 700 J $K^{-1}kg^{-1}$ are very similar to the results obtained in the reference simulations. On the other hand, the results when using a larger heat capacity produced wind speeds very different from the reference simulation. The mass stream function in Fig. 11(b), shows an atmosphere very different from the reference simulation at deep pressures. The difference is caused by a more convectively active atmosphere in the case of the simulation with 1100 J $K^{-1}kg^{-1}$.

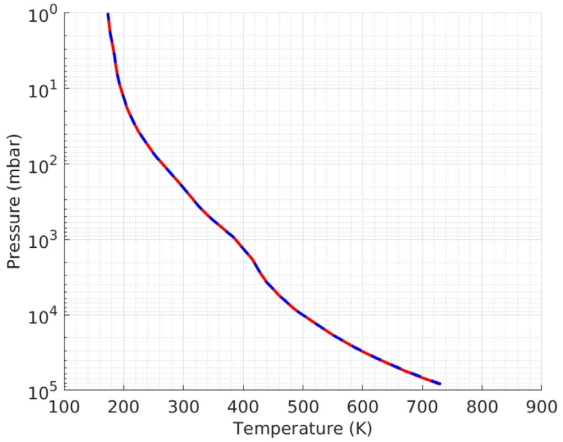

(a) Low surface friction experiment - Horizontally and time averaged temperatures

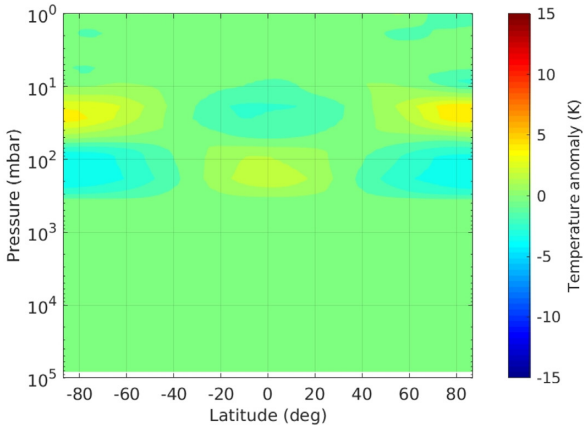

(b) Temperature anomaly maps

Figure 12. Temperatures obtained in the surface friction experiment ($k_f^{-1} = 10$ Earth day). (a) Map of the horizontally and time (1000 Earth days) averaged temperatures. The two colours correspond to the reference simulation with 4 deg spatial resolution (solid red line) and the low surface friction simulation (blue dashed line). (b) The zonal and time averaged (over 1000 Earth days) temperature anomaly maps.

The larger heat capacity allows the mixing in the atmosphere to be extended to larger atmospheric columns, which drags the horizontal motion. The mechanism accelerating the equator is a combination of zonal mean circulation, thermal tides, and transient waves (Mendonça et al. 2015), which is similar to the mechanism driving the atmospheric circulation in hot Jupiter planets (see e.g. Mayne et al. 2017). As shown in Zhang & Showman (2017), increasing the heat capacity can reduce the wave speed in the atmosphere, and disrupts the formation of a strong jet.

5.3 Surface friction

The physical properties of the planet's surface will be challenging to constrain through observations. However, the boundary layer has an important role representing a boundary condition that regulates, for example, the exchanges of heat and momentum between the surface and the atmosphere.

OASIS uses a very simplified boundary layer scheme as explained in Section 2, which linearly drags the winds in the boundary layer

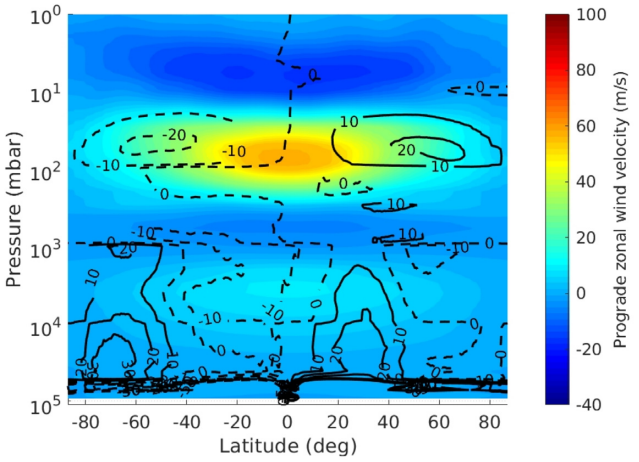

Figure 13. Zonally and timed averaged zonal winds and mass stream function for simulation with different lower surface friction ($k_f^{-1} = 10$ Earth days). This simulation uses 4 deg spatial resolution and the results averaged over 1000 Earth days. The units of the zonal winds are in $\mathrm{m\,s^{-1}}$ and the positive numbers point in the prograde direction of the planet. The mass stream function is in units of $10^{10}\ \mathrm{kg\,s^{-1}}$.

region. This parametrization is a very simple representation of the mechanical interaction between the surface and the atmosphere and it is controlled by a parameter that sets the strength of the surface friction. In this experiment, we reduce the strength of the friction and study its impact on the simulated atmosphere.

Figs 12 and 13 show the temperature and wind maps from the low friction experiment (surface friction 10× weaker than the reference simulation). The results obtained are almost identical to the reference simulation. The winds produced have a very important role driving in the temperature structure in Venus, like the temperature anomalies in latitude and small temperature differences in longitude. Since the lower surface friction does not have an important impact on the atmospheric winds produced, the temperatures obtained in this experiment are similar to the ones in the reference simulations.

6 VENUS SEEN AS AN EXOPLANET

OASIS is a theoretical tool capable of modelling the environment of planets and it can also be used to plan observations or build new ideas for observational methods. In this section, we explore our available tools to study the predicted spectral observations if the simulated planet of the previous sections (i.e. a Venus-like planet) were to be observed at a distance of 10 pc from Earth. Considering the characteristics of the planet–star system, we have focused on exploring the emission and reflected spectra of the planet. As we will see in the results below, a Venus-like planet around a Sun-like star will be possible to characterize with an observational facility such as the LUVOIR mission concept (The LUVOIR Team 2018). Our goal in this section is not to prove that a Venus-like planet can be observed by the LUVOIR mission concept, which has already been shown in The LUVOIR Team (2018), but to show that the new OASIS modules produce the expected observed spectra. Nevertheless, our results, as we show below are consistent with the results from The LUVOIR Team (2018).

In Fig. 14, we present the fluxes coming from the simulated planet, which include the emitted planet flux and the stellar radiation being reflected in the planet (obtained from the 3D simulations). The spectral resolution used in the figure is the same as the resolution

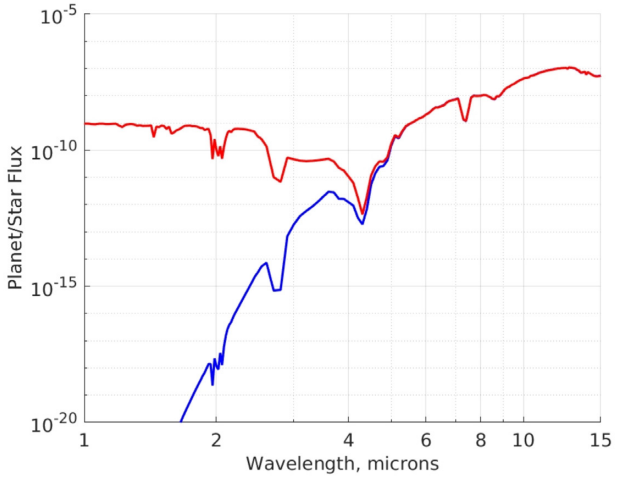

(a) Reference simulation

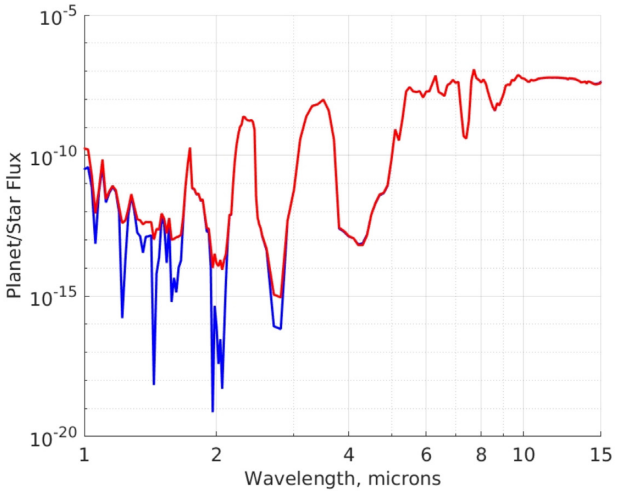

(b) Experiment with no clouds or extra UV absorption

Figure 14. Flux ratios for two simulations: (a) reference simulation and (b) experiment with no clouds and no extra UV absorption. The red lines correspond to the planet fluxes from the day-side of the planet and the blue lines to the night-side.

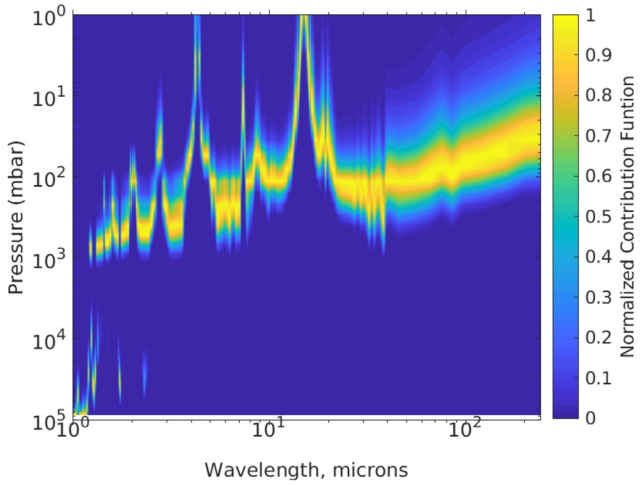

(a) Reference simulation

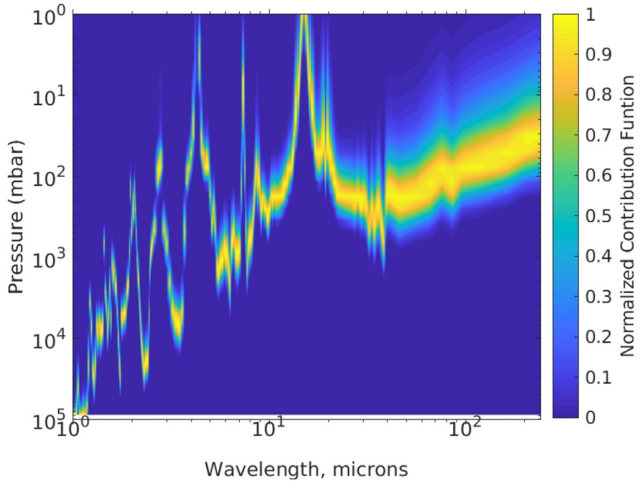

(b) Cloud free experiment

Figure 15. Contribution function as a function of wavelength for two simulations: reference and with no clouds.

used in the 3D simulations. In the figure, the two panels represent different simulations: (a) refers to the reference simulation and (b) refers to the simulation with no clouds and the unknown UV absorber. The coloured solid lines represent the flux coming from the day side (red) and night side (blue) of the planet. In the reference simulation, the impact of the clouds is very clear in the results shorter than 4 μm. The clouds are very reflective and help to significantly raise the outgoing flux. These results suggest that for a massive atmosphere such as the one in Venus, a highly reflective cloud structure helps raise the number of photons coming from the planet for wavelengths shorter than 4 μm, which otherwise would be absorbed in the deep atmosphere. In Fig. 14(a), there is a large contrast between the day and night sides of the planet, however, the differences decrease for wavelengths longer than 4 μm. At longer wavelengths the fluxes originate mostly from the upper atmosphere (above the clouds) where the atmospheric circulation has redistributed efficiently the heat and reduced the differences in temperature between the day- and night-side of the planet. In Section 3, we saw that the differences in temperature between the day and night side are relatively small. In Fig. 14(b), the spectrum shows stronger spectral signatures than in Fig. 14(a). These stronger signatures correspond to information from the lower atmosphere, which is now exposed due to the absence of the cloud structure. The fluxes are also higher due to the hotter deep atmosphere plus surface. The differences between the day–night side in the deep atmosphere (Fig. 14b) are mostly due to the differences in temperature between the two sides of the planet. The differences in temperature are caused by the winds being less efficient in mixing the heat in the deep atmosphere compared with the upper atmosphere. The contribution from the surface albedo (0.15) to the planet flux is very small.

The fluxes at different wavelength in Fig. 14 contain information from different regions in the atmosphere. A good diagnostic to explore from which pressure range the planet emission flux emerges is the contribution function. The contribution function (C_f) has the following form (Knutson et al. 2009):

$$C_f(p,\lambda) = B(\lambda,T)\mathrm{e}^{-\tau}\frac{\mathrm{d}\tau}{\mathrm{d}\log(p)}, \tag{8}$$

where the function B is the Planck function, T is the absolute temperature, τ is the optical depth, and p is the pressure. Fig. 15

Table 3. Instrument parameters used to simulate the possible spectrum obtained with LUVOIR. The formulation is based on Robinson, Stapelfeldt & Marley 2016.

Parameters	Value
Star radius (R_s)	1.0
Number of exozodis	1.0
Distance (pc)	10.0
Wavelength minimum (μm)	0.4
Wavelength maximum (μm)	2.5
Integration time (h)	10
Outer working angle (λ/D)	20.0
Raw contrast	10^{-10}
Instrument spectral resolution (λ/Δλ)	70
Telescope and instrument throughput	0.2
Dark current (s^{-1})	1×10^{-4}
Horizontal pixel spread of IFS spectrum	3
Read noise per pixel	0.1
Size of photometric aperture (λ/D)	1.5
Quantum efficiency	0.85
V-band zodiacal light surface brightness (mag arcsec^{-2} μm^{-}1)	23
V-band exozodiacal light surface brightness (mag arcsec^{-2} μm^{-}1)	22
Detector maximum exposure time (h)	1
Telescope mirror temperature (K)	80
Effective emissivity for the observing system (of order unity)	0.9

shows the contribution function for the reference simulation and the simulation with no clouds. As can be seen from the two panels, the cloud deck has an important impact shaping the contribution function. The main impact of the clouds is the block of the upward radiation coming from the deep layers for wavelengths shorter than 10 μm. Most of the emitted outgoing radiation at wavelengths shorter than 10 μm comes from the cloud deck at 1–0.1 bars. Note that the GCM resolves some spectral windows at wavelengths near 1 and 2 μm. Looking at these spectral windows, we can probe the extreme climate conditions of the deep atmosphere in the cloudy Venus (e.g. Allen & Crawford 1984). The peak shape features in the contribution function maps are related to the main absorption features of CO_2, for example at roughly: 1.6, 2, 2.7, 4.3, and 15 μm. For wavelengths longer than 10 μm, the emitted flux contributions are from pressure levels above the cloud base.

As shown in Fig. 14, in order to be able to observe a Venus analogue, our telescope needs to be able to resolve changes in the planet flux at the parts-per-billion (ppb) level or smaller. Mission concepts such as LUVOIR (The LUVOIR Team 2018) or HabEx (Gaudi et al. 2018) would make observations of Venus analogues feasible. Following the formalism developed in Robinson et al. (2016), we have written a module in the OASIS platform that allows us to simulate an observational spectrum using directly the results from the 3D simulations. Our observed spectra are based on a telescope that incorporates a coronograph. The main parameters of the instrument are listed in Table 3. In Fig. 16, we show the observed spectra at orbital phase 0.25 for different telescope diameters and 10 h of observation time. The Venus analogue was placed 10 pc away as for the results shown in the previous figure (Fig. 14). The spectral range observed is the same as the one proposed for the spectrograph in the LUVOIR concept mission. The instrument parameters are based on the work of Robinson et al. (2016). It is known that small inner working angles for the coronograph in a large telescope such as LUVOIR is challenging due to telescope

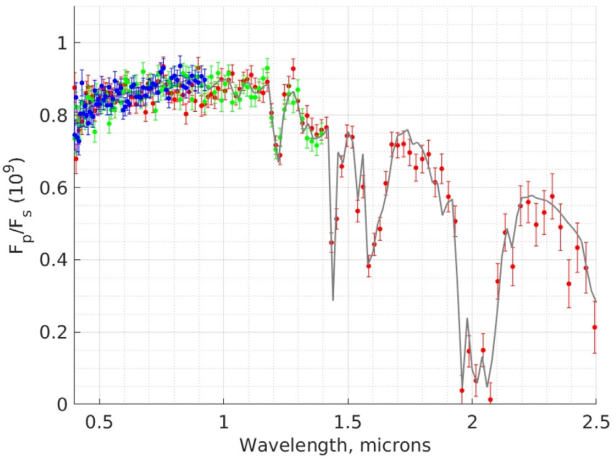

(a) Telescope diameter, 8 meters

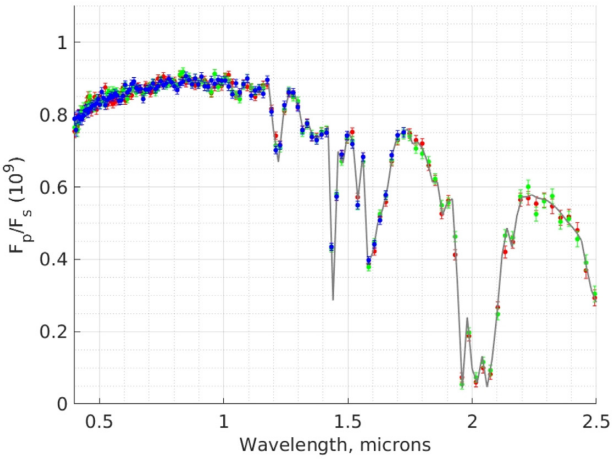

(b) Telescope diameter, 15 meters

Figure 16. Simulated spectral observation of a Venus analogue at 10 pc using a telescope with LUVOIR characteristics and an integration time of 10 h. The parameters used for the telescope are shown in Table 3. The black line represents the noise-free spectrum from the 3D simulation, and corresponds to the planet phase orbit 0.25. The two panels correspond to different sizes of the telescope diameter: (a) 8 m and (b) 15 m. The different point colours are the results of the simulated observations with different inner working angles of the coronograph: λ/D (red), 2λ/D (green), and 3λ/D (blue).

stability problems (Robinson et al. 2016). Additional information regarding the limitation of small angle coronographic techniques can be found in e.g. Mawet et al. (2012, 2014). However, a large inner working angle make the observations of planets close to the star difficult. Note that the inner working angle is proportional to λ/D, where *D* is the telescope diameter. As in Robinson et al. (2016), we have adopted the parameters for the near-IR detector that represent the HgCdTe detectors (see Table 3 and Morgan & Siegler 2015). In Fig. 16(a), we simulate the observations from an 8 m LUVOIR telescope with different inner working angles. The blue points represent an inner working angle of 3λ/D, which would only allow for observations at wavelengths shorter than 1 μm. It would be difficult to characterize the atmosphere from the data corresponding to the blue points, where the only information observed would be the reflected light from the cloud structure. With an inner working angle of 2λ/D (green points), we would be able to capture the H_2O feature

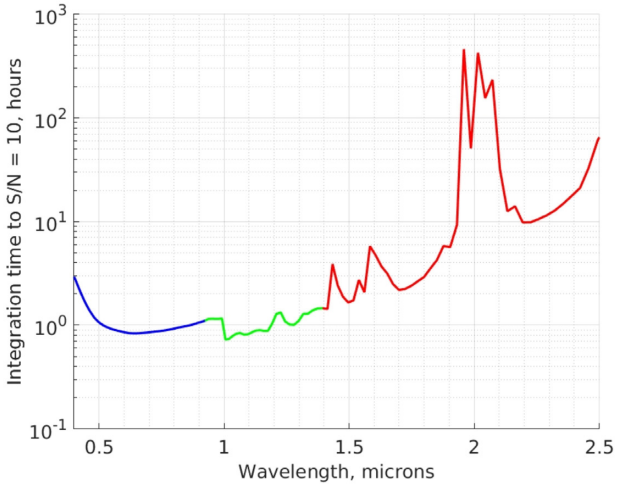

(a) Telescope diameter, 8 meters

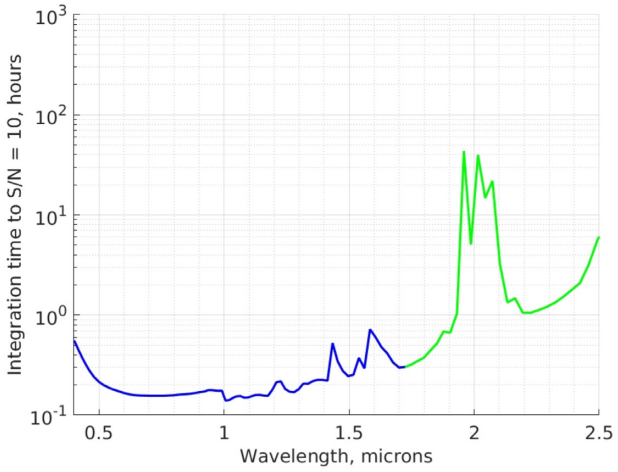

(b) Telescope diameter, 15 meters

Figure 17. Integration time for an S/N equal to 10. This figure uses the same parameters as in Fig. 16. The different panels correspond to telescopes with different diameter (a: 8 m; b: 15 m). The different line colours are the results of the simulated observations with different inner working angles of the coronograph: λ/D (red), 2λ/D (green), and 3λ/D (blue). Note that in panel (b), the red colour is not visible because it overlaps completely with the green line for this wavelength range (0.4–2.5 μm).

at roughly 1.2 μm. The red points represent an inner working angle of λ/D. By using this latter configuration in an 8 m telescope, we would be able to cover the instrument spectral range and capture the H_2O feature at 1.4 μm plus the CO_2 features at 1.6 and 2 μm. The information gathered from the observed spectrum would be able to constrain the upper atmosphere and cloud region. To reconstruct the global atmosphere based on the information obtained from the upper atmosphere, we would have to use theoretical models to make predictions on the deep atmospheric conditions. Fig. 16(b) shows that a 15 m diameter telescope would significantly improve the performance of the instrument, it would make it possible to observe the H_2O and CO_2 features with all the inner working angles tested. In Fig. 17, we show the roughly one order magnitude shorter time integration needed to acquire an S/N of 10 with a 15 m diameter telescope compared with the 8 m telescope. S/N is the signal-to-noise ratio defined by the ratio between the planet flux and the noise per spectral band. The maximum integration time

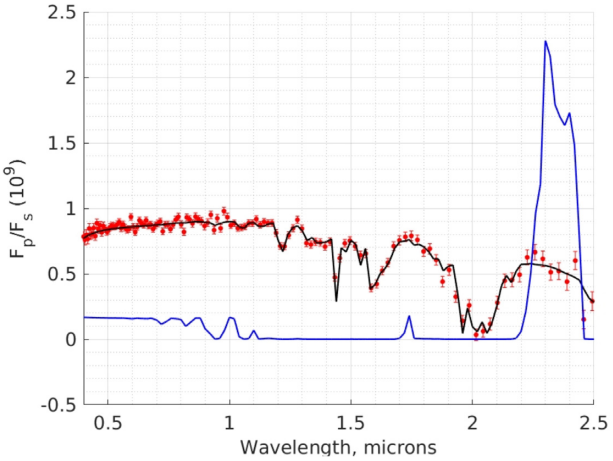

(a) Telescope diameter, 8 meters

Figure 18. Simulated spectral observation of a Venus analogue at 10 pc using an 8 m telescope with LUVOIR characteristics and an integration time of 10 h. The parameters used for the telescope are shown in Table 3. The black line represents the noise-free spectrum from the reference simulation and blue line from the cloud-free simulation, and both spectra correspond to the planet phase orbit 0.25. The inner working angles of the coronograph are defined as 3λ/D.

needed is roughly 40 h for the deep feature at 2 μm with the 15 m telescope.

Fig. 18 compares the spectrum of the reference simulation to the simulation with no clouds or unknown UV absorber, and shows that with the 8 m LUVOIR (and 10 h integration), it is possible to distinguish between a cloudy and a clear atmosphere. The highest peak in the clear atmosphere spectrum is due to the CO_2 emission from the hot deep layers, which in the cloudy atmosphere is absorbed at the cloud base.

7 CONCLUSIONS AND FUTURE PROSPECTS

The number of terrestrial planets discovered outside the Solar system with Earth-like masses and sizes continues to grow and there is a need of theoretical tools capable of characterizing the environment of these planets. We have developed a 3D platform, OASIS, capable of simulating the environment of terrestrial planets. The model has been developed from the ground up to avoid approximations that could hinder its flexibility to explore a large diversity of planetary conditions. The code has been developed using state-of-the-art programming techniques and GPUs, currently among the best hardware to power high performance computing. In this work, we have coupled the dynamics code (THOR) with the new radiation code (CYCLOPS), a simplified representation of surface and soil thermodynamics and physical properties (ATLANTIS), and convection and cascade of enstrophy (LOKI). The cloud and chemistry parameters were kept constant during the simulations.

OASIS has completed its first benchmark test, where the modules were combined to simulate a terrestrial planet. We decided to model a planet with Venus-like conditions, both for its inherent complexity and for its relevance for future exoplanet discoveries. It is important to explore Venus-like planets in the context of exoplanet research since they will inform us about the conditions of the inner boundary of the habitable zone. They are also important from an observational point of view since the transit method will be biased towards the detection of planets with orbits closer to the host stars than farther

away (Kane & von Braun 2008). The Venus environment is known to be technically and computationally difficult to simulate due to the complex optical structure of the atmosphere that requires a computationally expensive radiative transfer code coupled to a dynamical core to produce a robust 3D temperature structure and atmospheric circulation. Therefore, Venus provides a challenging case to test the capabilities of the current OASIS platform.

Our GPU implementation allowed us to use the radiation scheme with a fairly good spectral resolution in a GCM (353 spectral band and 20 Gaussian points for the *k*-distribution optical data). The new code performed robust simulations of the massive Venus atmosphere and is able to successfully reproduce an atmospheric circulation and temperature structure similar to the observations of Venus. This is an important achievement and shows that our model can confidently be used to explore Venus-like planets in the future. The winds in the upper cloud region obtained in the simulations with 2 deg resolution are as strong as indicated by the observations from cloud tracking measurements. Our 2 deg resolution simulation was able to simulate these strong winds with no fine tuning. The strong winds are part of a phenomenon called the 'superrotating' Venus atmosphere. We found that when using lower space resolution models, the winds in the cloud region are weaker than when using 2 deg resolution. The lower velocity wind values may be associated with the inaccuracies in the dynamical core when representing the angular momentum exchanges in the deep atmosphere for crude spatial resolutions (e.g. Lebonnois et al. 2012). Using higher spatial resolution helps reducing the numerical errors associated with the angular momentum in Venus simulations. With higher spatial resolution, such as 2 deg, these numerical errors become substantially smaller compared to the physical sources and transport of angular momentum in the simulated atmosphere, as we show here. The model finds a warmer cloud region than in the observations, but this is expected and caused by the cloud distribution used. We used such cloud distribution to be consistent with previous work (e.g. Lee & Richardson 2011).

We have also tested the impact of different model parameters on the atmospheric circulation and temperature. In summary, (i) when the clouds are removed, stellar energy is deposited deeper in the atmosphere leading to stronger atmospheric cells and weaker zonal winds. Removing the clouds also has an important impact on the temperature structure, where the surface temperature increases and produces a deep convective region represented by an adiabatic profile extending from the surface to pressure levels as high as 100 mbar; (ii) decreasing the heat capacity of the atmosphere to 700 J $K^{-1}kg^{-1}$ did not have a large impact on the simulated atmosphere. However, if the heat capacity is increased to 1100 J $K^{-1}kg^{-1}$ it has a large impact on the circulation produced, in the sense that the large-scale cells become stronger, but the low latitude jet weakens significantly. Both experiments produced temperature structures similar to the reference simulation, but the pole–equator differences are smaller in the case of higher heat capacity; and (iii) reducing the surface friction by one order of magnitude did not have a significant impact on the simulated atmosphere, which was largely similar to the reference simulation.

One of the goals of OASIS is to guide us in the preparation of observations. We showed the results of simulated spectra of a Venus analogue at 10 pc away from Earth as observed with a telescope similar to the LUVOIR mission concept. To be able to observe this planet–star system at 10 pc distance, we need to be able to reach values of planet/star contrasts of the order of 10^{-10}. The results show that it would be possible to characterize a Venus-like planet using LUVOIR, with a coronograph, a mirror of 8 m and an inner working angle of λ/D. These results are consistent with the results presented in The LUVOIR Team (2018). A specific configuration of the telescope diameter and the inner working angle of the coronograph is needed, and if the inner working angle is not sufficiently small, observations of Venus analogues will be almost impossible.

We have demonstrated that OASIS is capable of simulating terrestrial planet environments. As a platform, OASIS can be continuously updated by testing new algorithms and physical/chemical models to increase the sophistication and complexity of the platform.

ACKNOWLEDGEMENTS

We thank Sandra Raimundo and Tais Dahl for instructive conversations and comments on the manuscript. JM and LAB acknowledge financial support from the Villum Foundation YIP Program and the Carlsberg Foundation Distinguished Associate Professor Fellowship. The results of this work were computed in the new GPU cluster (FOUNDATION) supported by the DTU Space's strategic funds 2018.

REFERENCES

Abbot D. S., Pierrehumbert R. T., 2010, J. Geophys. Res.: Atmos., 115, D03104
Allen D. A., Crawford J. W., 1984, Nature, 307, 222
Anglada-Escudé G. et al., 2016, Nature, 536, 437
Baranov Y. I., Lafferty W. J., Fraser G. T., 2004, J. Mol. Spectrosc., 228, 432
Batalha N. E., Lewis N. K., Line M. R., Valenti J., Stevenson K., 2018, ApJ, 856, L34
Bézard B., Fedorova A., Bertaux J.-L., Rodin A., Korablev O., 2011, Icarus, 216, 173
Bonfils X. et al., 2018, A&A, 613, A25
Bullock M. A., Grinspoon D. H., 2001, Icarus, 150, 19
Caldas A., Leconte J., Selsis F., Waldmann I. P., Bordé P., Rocchetto M., Charnay B., 2019, A&A, 623, A161
Carpenter R. L., 1964, AJ, 69, 2
Catling D. C., Kasting J. F., 2017, Atmospheric Evolution on Inhabited and Lifeless Worlds. Cambridge Univ. Press, New York
Charnay B., Forget F., Wordsworth R., Leconte J., Millour E., Codron F., Spiga A., 2013, J. Geophys. Res.: Atmos., 118, 10414
Charnay B., Barth E., Rafkin S., Narteau C., Lebonnois S., Rodriguez S., Courrech Du Pont S., Lucas A., 2015, Nat. Geosci., 8, 362
Crisp D., 1986, Icarus, 67, 484
Crisp D., 1989, Icarus, 77, 391
de Bergh C., Bezard B., Crisp D., Maillard J. P., Owen T., Pollack J., Grinspoon D., 1995, Adv. Space. Res., 15, 79
Deitrick R., Mendonça J. M., Schroffenegger U., Grimm S. L., Tsai S.-M., Heng K., 2020, ApJS, 248, 30
Del Genio A. D., Way M. J., Amundsen D. S., Aleinov I., Kelley M., Kiang N. Y., Clune T. L., 2019, Astrobiology, 19, 99
Dittmann J. A. et al., 2017, Nature, 544, 333
Donner L. J., Large W. G., 2008, Annu. Rev. Environ. Resour., 33, 1
Dressing C. D., Charbonneau D., 2015, ApJ, 807, 45
Eymet V., Fournier R., Dufresne J., Lebonnois S., Hourdin F., Bullock M. A., 2009, J. Geophys. Res., 114, E11008
Fisher C., Heng K., 2018, MNRAS, 481, 4698
Forget F., 2013, Int. J. Astrobiol., 12, 177
Forget F. et al., 1999, J. Geophys. Res., 104, 24155
Forget F., Bertrand T., Vangvichith M., Leconte J., Millour E., Lellouch E., 2017, Icarus, 287, 54
Frandsen B. N., Wennberg P. O., Kjaergaard H. G., 2016, Geophys. Res. Lett., 43, 11
Gamache R. R. et al., 2017, J. Quant. Spectrosc. Radiat. Transfer, 203, 70

Gaudi B. S. et al., 2018, preprint (arxiv:1809.09674)
Gillon M. et al., 2016, Nature, 533, 221
Gillon M. et al., 2017, Nature, 542, 456
Goldstein R. M., 1964, AJ, 69, 12
Grimm S. L., Heng K., 2015, ApJ, 808, 182
Gruszka M., Borysow A., 1997, Icarus, 129, 172
Haqq-Misra J., Wolf E. T., Joshi M., Zhang X., Kopparapu R. K., 2018, ApJ, 852, 67
Haus R., Kappel D., Arnold G., 2015, Planet. Space Sci., 117, 262
Held I. M., Suarez M. J., 1994, Bull. Am. Meteorol. Soc., 75, 1825
Hourdin F., Le van P., Forget F., Talagrand O., 1993, J. Atmos. Sci., 50, 3625
Ingersoll A. P., 1969, J. Atmos. Sci., 26, 1191
Kane S. R., von Braun K., 2008, ApJ, 689, 492
Kane S. R., Kopparapu R. K., Domagal-Goldman S. D., 2014, ApJ, 794, L5
Kerzhanovich V. V., Limaye S. S., 1985, Adv. Space. Res., 5, 59
Kliore A. J., Moroz V. I., Keating G. M., 1985, Adv. Space Res., 5, 1
Knollenberg R. G., Hunten D. M., 1980, J. Geophys. Res., 85, 8039
Knutson H. A. et al., 2009, ApJ, 690, 822
Komacek T. D., Abbot D. S., 2019, ApJ, 871, 245
Kopparapu R. k., Wolf E. T., Haqq-Misra J., Yang J., Kasting J. F., Meadows V., Terrien R., Mahadevan S., 2016, ApJ, 819, 84
Krasnopolsky V. A., 2017, Icarus, 286, 134
Lacis A. A., Oinas V., 1991, J. Geophys. Res., 96, 9027
Lavie B. et al., 2017, AJ, 154, 91
Lebonnois S., Hourdin F., Eymet V., Crespin A., Fournier R., Forget F., 2010, J. Geophys. Res., 115, E06006
Lebonnois S., Covey C., Grossman A., Parish H., Schubert G., Walterscheid R., Lauritzen P., Jablonowski C., 2012, J. Geophys. Res., 117, E12004
Lebonnois S., Eymet V., Lee C., Vatant d'Ollone J., 2015, J. Geophys. Res., 120, 1186
Lebonnois S., Sugimoto N., Gilli G., 2016, Icarus, 278, 38
Lebrun T., Massol H., ChassefièRe E., Davaille A., Marcq E., Sarda P., Leblanc F., Brandeis G., 2013, J. Geophys. Res., 118, 1155
Leconte J., Forget F., Charnay B., Wordsworth R., Pottier A., 2013, Nature, 504, 268
Lee C., Richardson M. I., 2011, J. Atmos. Sci., 68, 1323
Lee C., Lewis S. R., Read P. L., 2007, J. Geophys. Res., 112, E04S11
Leovy C. B., 1973, J. Atmos. Sci., 30, 1218
Limaye S. S., Mogul R., Smith D. J., Ansari A. H., Słowik G. P., Vaishampayan P., 2018, Astrobiology, 18, 1181
Lincowski A. P., Meadows V. S., Crisp D., Robinson T. D., Luger R., Lustig-Yaeger J., Arney G. N., 2018, ApJ, 867, 76
Luger R. et al., 2017, Nat. Astron., 1, 0129
Lustig-Yaeger J., Meadows V. S., Lincowski A. P., 2019, AJ, 158, 27
Malik M. et al., 2017, AJ, 153, 56
Malik M., Kitzmann D., Mendonça J. M., Grimm S. L., Marleau G.-D., Linder E. F., Tsai S.-M., Heng K., 2019, AJ, 157, 170
Marcq E., Encrenaz T., Bézard B., Birlan M., 2006, Planet. Space Sci., 54, 1360
Mawet D. et al., 2012, in Clampin M. C., Fazio G. G., MacEwen H. A., Oschmann J. M., eds, Proc. SPIE Conf. Ser. Vol. 8442, Space Telescopes and Instrumentation 2012: Optical, Infrared, and Millimeter Wave. SPIE, Bellingham, p. 844204
Mawet D. et al., 2014, ApJ, 792, 97
Mayne N. J. et al., 2017, A&A, 604, A79
Meadows V. S., Crisp D., 1996, J. Geophys. Res., 101, 4595
Mendonça J. M., Read P. L., 2016, Planet. Space Sci., 134, 1
Mendonça J. M., Read P. L., Wilson C. F., Lewis S. R., 2012, Icarus, 217, 629
Mendonça J. M., Read P. L., Wilson C. F., Lee C., 2015, Planet. Space Sci., 105, 80
Mendonça J. M., Grimm S. L., Grosheintz L., Heng K., 2016, ApJ, 829, 115
Mendonça J. M., Tsai S.-M., Malik M., Grimm S. L., Heng K., 2018, ApJ, 869, 107
Morgan R., Siegler N., 2015, Proc. SPIE, 9605, 96052I
Morley C. V., Kreidberg L., Rustamkulov Z., Robinson T., Fortney J. J., 2017, ApJ, 850, 121
Palmer K. F., Williams D., 1975, Appl. Opt., 14, 208
Pieters C. M., Head J. W., Patterson W., Pratt S., Garvin J., 1986, Science, 234, 1379
Read P. L., 1986, Q. J. R. Meteorol. Soc., 112, 253
Read P. L. et al., 2016, Q. J. R. Meteorol. Soc., 142, 703
Read P. L. et al., 2017, in Haberle R. M. et al., The Martian Planetary Boundary Layer. Cambridge Univ. Press, Cambridge, p. 106
Rees G., 1999, The Remote Sensing Data Book. Cambridge Univ. Press, Cambridge, New York, p. 262
Robinson T. D., Catling D. C., 2012, ApJ, 757, 104
Robinson T. D., Stapelfeldt K. R., Marley M. S., 2016, PASP, 128, 025003
Sagan C., 1961, Science, 133, 849
Sánchez-Lavega A., Lebonnois S., Imamura T., Read P., Luz D., 2017, Space Sci. Rev., 212, 1541
Satoh M., 2002, Mon. Weather Rev., 130, 1227
Shields A. L., 2019, ApJS, 243, 30
Shields A. L., Barnes R., Agol E., Charnay B., Bitz C., Meadows V. S., 2016, Astrobiology, 16, 443
Stamnes K., Tsay S., Wiscombe W., Laszlo I., 2000, Rep. available from ftp://climatel.gsfc.nasa.gov.wiscombe
Taylor F. W., Svedhem H., Head J. W., 2018, Space Sci. Rev., 214, 35
Tellmann S., Pätzold M., Häusler B., Bird M. K., Tyler G. L., 2009, J. Geophys. Res., 114, E00B36
The LUVOIR Team, 2018, preprint (arxiv:1809.09668)
Thuburn J., 2008, J. Comput. Phys., 227, 3715
Tomasko M. G., Doose L. R., Smith P. H., Odell A. P., 1980, J. Geophys. Res., 85, 8167
Tsai S.-M., Lyons J. R., Grosheintz L., Rimmer P. B., Kitzmann D., Heng K., 2017, ApJS, 228, 20
Turbet M., Forget F., Leconte J., Charnay B., Tobie G., 2017, Earth Planet. Sci. Lett., 476, 11
von Zahn U., Moroz V. I., 1985, Adv. Space. Res., 5, 173
Warrilow D. A., Sangster A. B., Slingo A., 1986, Tech. Rep. DCTN 38, UKMO, UK
Wolf E. T., Toon O. B., 2013, Astrobiology, 13, 656
Wordsworth R., 2015, ApJ, 806, 180
Wordsworth R. D., Forget F., Selsis F., Millour E., Charnay B., Madeleine J.-B., 2011, ApJ, 733, L48
Wordsworth R., Kalugina Y., Lokshtanov S., Vigasin A., Ehlmann B., Head J., Sanders C., Wang H., 2017, Geophys. Res. Lett., 44, 665
Wunderlich F. et al., 2019, A&A, 624, A49
Yang J., Abbot D. S., Koll D. D. B., Hu Y., Showman A. P., 2019, ApJ, 871, 29
Zasova L. V., Moroz V. I., Formisano V., Ignatiev N. I., Khatuntsev I. V., 2004, Adv. Space. Res., 34, 1655
Zhang X., Showman A. P., 2017, ApJ, 836, 73

This paper has been typeset from a TEX/LATEX file prepared by the author.